NAVAL POSTGRADUATE SCHOOL

MONTEREY, CALIFORNIA

THESIS

PHASE DIVERSITY WAVEFRONT SENSING FOR CONTROL OF SPACE BASED ADAPTIVE OPTICS SYSTEMS

by

Richard J Schgallis

December 2007

Thesis Advisor:	Brij Agrawal
Co-Advisor:	Andres Larraza
Second Reader:	Jae-Jun Kim

Approved for public release; distribution is unlimited

THIS PAGE INTENTIONALLY LEFT BLANK

REPORT DOCUMENTATION PAGE			Form Approved OMB No. 0704-0188
Public reporting burden for this collection of information is estimated to average 1 hour per response, including the time for reviewing instruction, searching existing data sources, gathering and maintaining the data needed, and completing and reviewing the collection of information. Send comments regarding this burden estimate or any other aspect of this collection of information, including suggestions for reducing this burden, to Washington headquarters Services, Directorate for Information Operations and Reports, 1215 Jefferson Davis Highway, Suite 1204, Arlington, VA 22202-4302, and to the Office of Management and Budget, Paperwork Reduction Project (0704-0188) Washington DC 20503.			
1. AGENCY USE ONLY *(Leave blank)*	**2. REPORT DATE** December 2007	**3. REPORT TYPE AND DATES COVERED** Master's Thesis	
4. TITLE AND SUBTITLE Phase Diversity Wavefront Sensing for Control of Space Based Adaptive Optics Systems			**5. FUNDING NUMBERS**
6. AUTHOR(S) Richard J Schgallis			
7. PERFORMING ORGANIZATION NAME(S) AND ADDRESS(ES) Naval Postgraduate School Monterey, CA 93943-5000			**8. PERFORMING ORGANIZATION REPORT NUMBER**
9. SPONSORING /MONITORING AGENCY NAME(S) AND ADDRESS(ES) N/A			**10. SPONSORING/MONITORING AGENCY REPORT NUMBER**
11. SUPPLEMENTARY NOTES The views expressed in this thesis are those of the author and do not reflect the official policy or position of the Department of Defense or the U.S. Government.			
12a. DISTRIBUTION / AVAILABILITY STATEMENT Approved for public release; distribution is unlimited			**12b. DISTRIBUTION CODE**

13. ABSTRACT (maximum 200 words)

Phase Diversity Wavefront Sensing (PD WFS) is a wavefront reconstruction technique used in adaptive optics, which takes advantage of the curvature conjugating analog physical properties of a deformable mirror (MMDM or Bi-morph) such that the computational intensity required for correcting an aberrated wavefront, becomes simplified over traditional Shack-Hartmann WFS techniques. By looking at an image reflected off a deformable mirror by two cameras placed on either side of focus of a lens, intensity differences, indicating wavefront aberration in the beam, can be detected by the cameras acting together as a WFS and analyzed by a computer providing control to the actuators of a deformable mirror such that any detected difference in intensities between the two cameras can be minimized. This process of mirror surface conjugation serves to correct for the aberrated or curved wavefront by reflecting a new wavefront, compensated for curvature, such that its reflection is approximately planar.

The theory of PD WFS is well documented however, there is very little quantifiable information regarding the specific challenges in designing a functioning PD WFS. In this research a PD WFS was designed and the concept proven such that a wavefront could be corrected through a computer controlled closed loop conjugation of a deformable mirror. The results were analyzed using a traditional Shack-Hartmann WFS and off-the-shelf "Front Surfer" wavefront analysis software to verify the validity of the experimental data.

PD WFS has become critical in the development of segmented mirror adaptive optical systems where traditional wavefront reconstruction using Shack-Hartmann wavefront sensing tends to break down at the mirror segment edges. The Naval Postgraduate School, Spacecraft Research and Design Center (SRDC) intends to explore the use of a segmented mirror adaptive optical systems for space based applications.

14. SUBJECT TERMS Adaptive Optics, Wavefront Sensor, Wave Front Sensor, Phase Diversity, Shack Hartmann			**15. NUMBER OF PAGES** 71
			16. PRICE CODE
17. SECURITY CLASSIFICATION OF REPORT Unclassified	**18. SECURITY CLASSIFICATION OF THIS PAGE** Unclassified	**19. SECURITY CLASSIFICATION OF ABSTRACT** Unclassified	**20. LIMITATION OF ABSTRACT** UU

NSN 7540-01-280-5500 Standard Form 298 (Rev. 2-89)

THIS PAGE INTENTIONALLY LEFT BLANK

Approved for public release; distribution is unlimited

PHASE DIVERSITY WAVEFRONT SENSING FOR CONTROL OF SPACE BASED ADAPTIVE OPTICS SYSTEMS

Richard J Schgallis
Commander, United States Navy
B.S., Jacksonville University, 1991
MBA, University of West Florida, 2001

Submitted in partial fulfillment of the
requirements for the degree of

MASTER OF SCIENCE IN APPLIED PHYSICS

from the

NAVAL POSTGRADUATE SCHOOL
December 2007

Author: Richard J Schgallis

Approved by: Dr. Brij Agrawal
Thesis Advisor

Dr. Andres Larraza
Co-Advisor

Dr. Jae-Jun Kim
Second Reader

Dr. James Luscombe
Chairman, Department of Physics

THIS PAGE INTENTIONALLY LEFT BLANK

ABSTRACT

Phase Diversity Wavefront Sensing (PD WFS) is a wavefront reconstruction technique used in adaptive optics, which takes advantage of the curvature conjugating analog physical properties of a deformable mirror (MMDM or Bi-morph) such that the computational intensity required for correcting an aberrated wavefront, becomes simplified over traditional Shack-Hartmann WFS techniques. By looking at an image reflected off a deformable mirror by two cameras placed on either side of focus of a lens, intensity differences, indicating wavefront aberration in the beam, can be detected by the cameras acting together as a WFS and analyzed by a computer providing control to the actuators of a deformable mirror such that any detected difference in intensities between the two cameras can be minimized. This process of mirror surface conjugation serves to correct for the aberrated or curved wavefront by reflecting a new wavefront, compensated for curvature, such that its reflection is approximately planar.

The theory of PD WFS is well documented however, there is very little quantifiable information regarding the specific challenges in designing a functioning PD WFS. In this research a PD WFS was designed and the concept proven such that a wavefront could be corrected through a computer controlled closed loop conjugation of a deformable mirror. The results were analyzed using a traditional Shack-Hartmann WFS and off-the-shelf “Front Surfer” wavefront analysis software to verify the validity of the experimental data.

PD WFS has become critical in the development of segmented mirror adaptive optical systems where traditional wavefront reconstruction using Shack-Hartmann wavefront sensing tends to break down at the mirror segment edges. The Naval Postgraduate School, Spacecraft Research and Design Center (SRDC) intends to explore the use of a segmented mirror adaptive optical systems for space based applications.

THIS PAGE INTENTIONALLY LEFT BLANK

TABLE OF CONTENTS

THIS PAGE INTENTIONALLY LEFT BLANK

LIST OF FIGURES

LIST OF TABLES

THIS PAGE INTENTIONALLY LEFT BLANK

ACKNOWLEDGMENTS

I would like to express my sincerest thanks to Distinguished Professor Brij Agrawal who so generously provided me with the resources to undertake this research. Professor your commitment to not only higher education but to the care and mentoring of individual students is beyond compare.

I similarly would like to thank Dr. Ty Martinez, Dr. Sergio Restaino and Jonathan Andrews of the Naval Research Laboratory, Albuquerque, NM for their selfless dedication in support of time and expertise for this endeavor. This project would not have succeeded without your steadfast devotion to student education and collective patience of saints.

Additionally, I would like to express my sincerest gratitude to Astronaut Jim Newman, and Dr. Jae-Jun Kim for their willingness to jump in and lend a hand in putting the pieces together in the 11th hour. The fact that you both would be so generous in spending untold hours on my behalf and out of sheer generosity speaks volumes for your selfless character. I am honored to have such outstanding mentors and friends.

To CAPT Al Scott, the finest naval officer I have ever met. Thank you, sir for all you've done for me during my tenure here. I have grown so much from your professional mentorship and can only hope that one day I can take the lessons in leadership you've taught me through your example, and apply them to help the next generation of Naval Space Cadre Officers.

Finally, I must dedicate this thesis to my wife and three boys, Richard, Jackson and Paddy for allowing Papa to work late almost daily for the last 33 months in order to finish this degree. I love you with all my heart!

THIS PAGE INTENTIONALLY LEFT BLANK

I. INTRODUCTION

Optics used to resolve images, regardless of wavelength, provide only a best estimation of the image assuming the light received from the image / source is uniform and undisturbed through the transmission medium. As a result, resolved images have error stemming from aberrations in the wavefront routinely caused by atmospheric turbulence, transmitter or detector jitter, or simple aberrations in the optical system itself; all of which will affect image quality. Routinely, these errors are insignificant and can be ignored, however there are many applications such as laser communications (pointing control), and terrestrial-based deep-space or high-resolution observations, where these errors need all possible compensation in order to facilitate resolution qualities necessary for the given purpose.

To achieve these purposes, Adaptive Optical systems can be utilized to detect and compensate for an aberrated wavefront, by applying corrections to the optical system such that the detector receives a best approximation of the original wavefront. In order to correct for aberration in a wavefront with an Adaptive Optics (AO) system, the required components consist of a wavefront sensor, deformable mirror and a computer which can evaluate the sensed wavefront, then make corrections to the deformable mirror before the process starts anew. Figure 1 shows how these components can be integrated into an AO system to correct for an aberrated image or wavefront.

The wavefront sensor detects the aberrated wavefront intensity using a multitude of sensors arranged in a grid or screen capable detecting changes in the intensity from point-to-point across the detector surface or in the case of phase diversity sensing, detects changes in intensity from one detector to another.

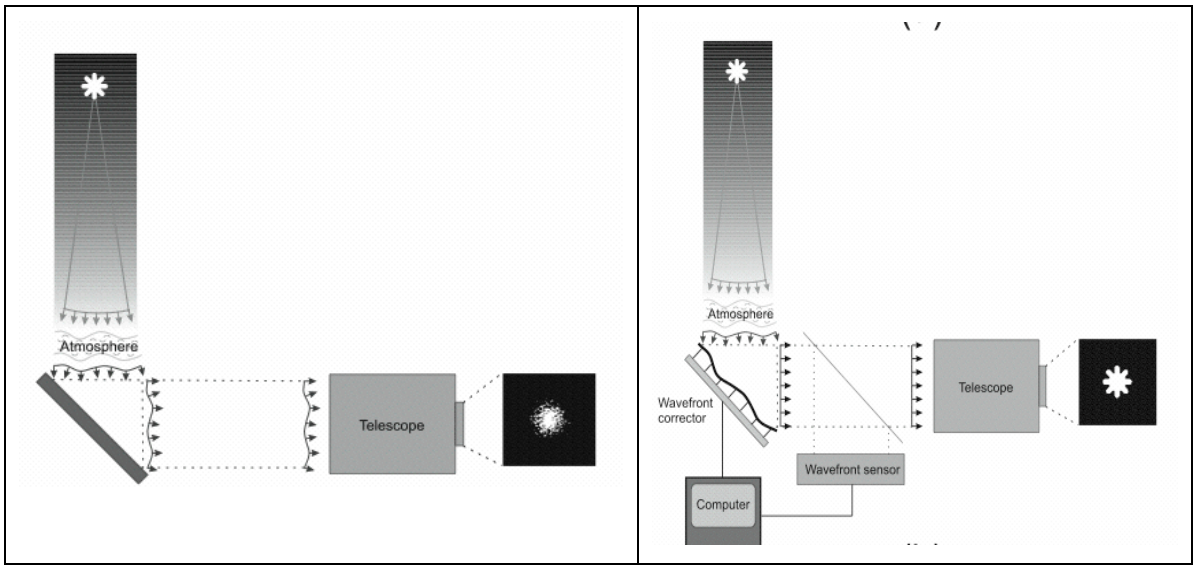

Figure 1 Left showing aberrated light or wavefront incident on a planar mirror and resolving through optics (telescope) an aberrated image. Right showing the aberrated light incident on a deformable mirror conjugated by computer interface with a wavefront sensor, in order to match the curvature or shape of the wavefront such that the image is corrected for the aberrations. Images courtesy of OKO Adaptive Optics Product Guide.

Knowing that the intensity of the unaberrated wavefront takes on a uniform Gaussian shape, a computer can analyze the intensity differences in an aberrated wavefront using a wavefront sensor and then compute a best approximation difference between the detected intensity and the ideal Gaussian. The computer then applies a conjugate correction to a deformable mirror to compensate for this error by applying voltage to each of the deformable mirror's actuators in attempts at full or partial conjugation of the wavefront.

The Deformable Mirror is a mirror whose surface can be manipulated such that changes in the shape of the surface can be used to compensate for the aberrated wavefront by reconstructing it to its natural Gaussian shape. This is done by conjugation which is simply an attempt to match the shape of the wavefront with the mirror surface before the actual wavefront arrives at the mirror surface. In order to accomplish this accurately, computational speed must be faster than that which is causing disturbances to

the wavefront**.** Figure 2 shows an aberrated image on the left and the same image corrected by a deformable mirror adaptive optics system on the right.

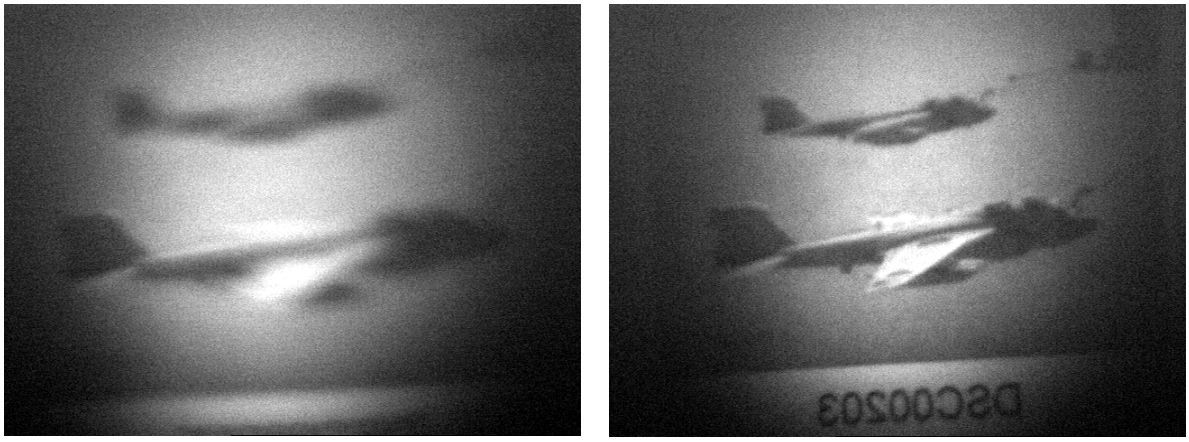

Figure 2 An aberrated image on the left and the same image corrected by a deformable mirror adaptive optics system on the right.

A. SCOPE OF RESEARCH

The Naval Postgraduate School Spacecraft Research and Design Center (SRDC) is researching in the field of Acquisition Tracking and Pointing (ATP) for space based applications. The work undertaken within the SRDC comprises jitter control, optics, control optimization, adaptive optics, and ATP for a myriad of electromagnetic spectrum applications ranging from relay laser communications, to optical system slewing, to future on orbit capabilities with large light weight optical systems capable of high fidelity terrestrial viewing from geosynchronous orbits. This work is part of a much larger effort geared towards the latter objective.

The objectives for this research were to build a Phase Diversity Wavefront Sensing system and develop a basic closed loop control algorithm necessary to conjugate a deformable mirror to correct for an aberrated wavefront using the data collected from the sensor. Finally, using off the shelf wavefront analysis software and hardware, evaluate the performance and versatility of the developed system.

THIS PAGE INTENTIONALLY LEFT BLANK

II. BACKGROUND

A. THE WAVEFRONT

In order to fully understand the science of Adaptive Optics, one must first understand the physics of the wavefront. First we will derive the Wave Equation starting from Maxwell's Equations.

$$\nabla \bullet E = \rho / \varepsilon_0 \tag{2.1}$$

$$\nabla \bullet B = 0 \tag{2.2}$$

$$\nabla \times E = -\partial B / \partial t \tag{2.3}$$

$$\nabla \times B = \mu_0 J + \mu_0 \varepsilon_0 \partial E / \partial t \tag{2.4}$$

Where E is the Electric Field Strength, B is the Magnetic Flux Density, ρ is the Density of Electric Charge, J is the Current Density, μ_0 is the Permeability of Free Space and ε_0 is the Permittivity of Free Space.

Taking the curl of equation (2.3):

$$\nabla \times (\nabla \times E) = -\nabla \times \partial B / \partial t \tag{2.5}$$

Now, taking the derivative of equation (2.4), in the case where J=0 (no charge or current).

$$\partial / \partial t(\nabla \times B) = \mu_0 \varepsilon_0 \partial / \partial t(\partial E / \partial t) = \mu_0 \varepsilon_0 (\partial^2 E / \partial t^2) \tag{2.6}$$

Where $\partial / \partial t(\mu_0 J) = 0$

Replacing $\nabla \times \partial B / \partial t$ in equation (2.5) with the term obtained in (2.6) we have:

$$\nabla \times (\nabla \times E) = -\nabla \times \partial B / \partial t = -\partial / \partial t(\nabla \times B) = -\mu_0 \varepsilon_0 (\partial^2 E / \partial t^2) \tag{2.7}$$

Now using the vector identity to recast the equation: $\nabla \times (\nabla \times A) = \nabla(\nabla \bullet A) - \nabla^2 A$

$$\nabla(\nabla \bullet E) - \nabla^2 E = -\mu_0 \varepsilon_0 (\partial^2 E / \partial t^2) \tag{2.8}$$

Using Poisson's equation the divergence of E =0 and we are left with;

$$\nabla^2 E - \mu_0 \varepsilon_0 (\partial^2 E / \partial t^2) = 0 \qquad (2.9)$$

This is the Wave Equation and it governs the properties of a propagating wave. Note this equation holds regardless of whether dealing with an Electric or Magnetic field wave. Since E and B, are interchangeable in the field sense, convention uses a U to denote either.

Therefore: $$\nabla^2 U - \mu_0 \varepsilon_0 (\partial^2 U / \partial t^2) = 0 \qquad (2.10)$$

Finally, and leaving the math for a future discussion: Using the Helmholtz Equation with Green's Theorem, solving the differential equation gives:

$$U(x, y, z, t) = \mathrm{Re} U_0(x, y, z, t) e^{-i\omega t} \qquad (2.11)$$

With the functional form of the propagating wave in hand we turn to the Huygens-Fresnel principle for spherically expanding waves. This is the well established principle that every unobstructed point on the surface of a wavefront serves as a source of spherical secondary wavelets (with the same frequency as that of the primary wave). (Hecht, E. 2001)

Furthermore we know from the principles of diffraction that this wavefront passing through any aperture such as a lens in our optical system will cause a diffraction pattern in the intensity of the wave. It is this intensity which is the metric which can be evaluated such that the wavefront can be measured. Figure 3 shows a diagram of an unaberrated wavefront diffracting though a focusing element (lens) and representation of it 1-D intensity function $(\mathrm{sinc})^2$ function.

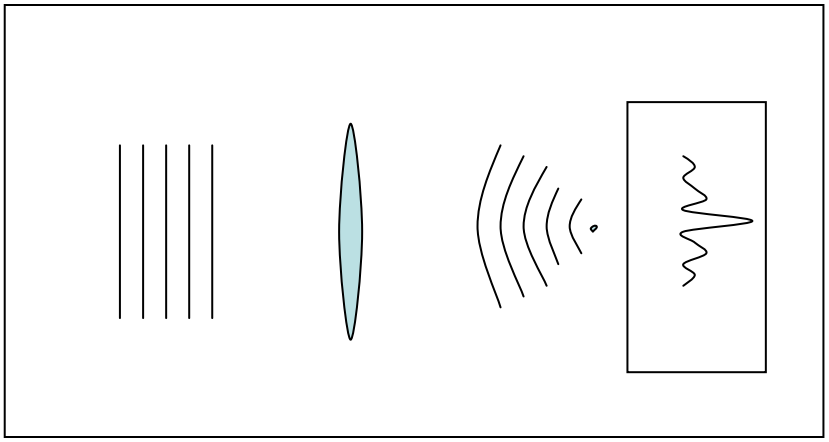

Figure 3 Unaberrated wavefront through a lens.

1. Wavefront Correction

In order for an aberrated wavefront to be corrected back to a planar wavefront, a method of conjugation of a mirror surface is used. This is a process by which a mirror shape is morphed to mimic the surface of the wavefront itself. It is important to note here that due to travel time of the wave through reflection, it is necessary to morph the surface of the mirror in amplitude differences of ½ of that of the actual wavefront and that the reflected wavefront will maintain some subtle hints of diffraction from discontinuities in the mirror surface. A simplistic example of this process is shown below.

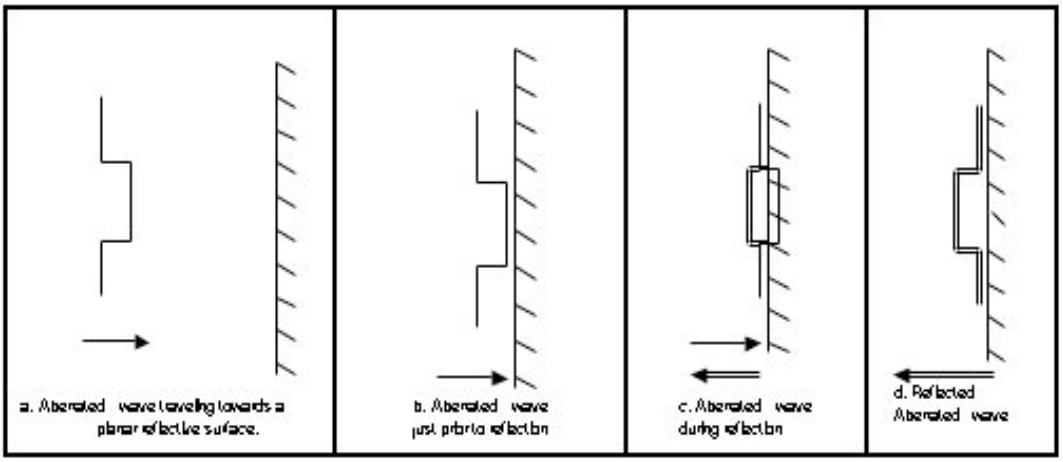

Figure 4 An aberrated wave reflects off a planar mirror surface. (Tyson, R. K. 1998)

In Figure 5 an aberrated wave reflects off a conjugated mirror surface reflecting a reconstructed (planar) wavefront. (Note the conjugated mirror amplitude is approx ½ of that of the wavefront in order to compensate for 2 times the leading edge travel time of the front edge of the wavefront. (Tyson R. K. 1998)

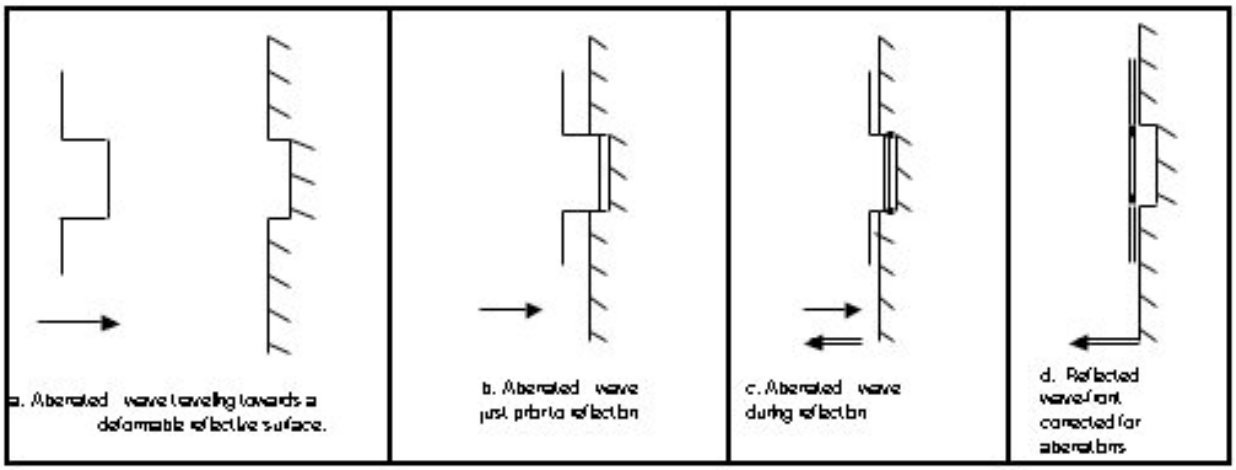

Figure 5 Aberrated wave reflecting off a conjugating surface and returning unaberrated. (Tyson, R. K. 1998)

B. THE WAVEFRONT SENSOR

Wavefront sensors play an important role in the process of reconstructing a wavefront. It is the role of the sensor to determine the nature of the aberration affecting the wavefront. This nature is quantified by comparison with a known reference unaberrated wavefront. The difference between the observed (aberrated) wavefront and a reference (unaberrated) wavefront is computed and corrective differences are made to the deformable mirror such that the wavefront can be measured again and the processing loop proceeds on while in each iteration, reducing the difference between corrected and reference beams. The two most widely used wavefront sensors are, the Shack-Hartmann and the Phase Diversity wavefront sensor.

1. Shack Hartmann

The Shack-Hartmann Wavefront Sensor measures wavefront slopes (the change in focus position) from one sub-aperture of the WFS to the next. Simply, an image of the exit pupil is projected onto a group of identical lenslets. Each lenslet takes a small part of the aperture, called a sub-pupil, and forms an image of the source. All the images are then formed on the same detector, typically a CCD. When an incoming wavefront is planar, all images are located in a regular grid defined by the lenslet array geometry. If the wavefront is distorted, the images become displaced from their nominal positions. These displacements of the image centroids are proportional to the average of the wavefront slopes. The wavefront itself is reconstructed from the arrays of measured slopes. (CFAO, 2007)

In Figure 6 we see a depiction of the Shack-Hartmann WFS. The top image shows the image received from a non-aberrated wavefront. Notice the uniform arrangement of lenslet focus centroids. This, in effect forms the reference patters from which the aberrated wavefront can be compared. The second depiction of an aberrated wave shows how the uniform pattern is lost but though a mathematical control algorithm, a deformable mirror can be commanded to conjugate its surface and thus reconstruct the geometrical array based on the assumptions that the individual displacements do not exceed the limitations of the WFS. (CFAO, 2007)

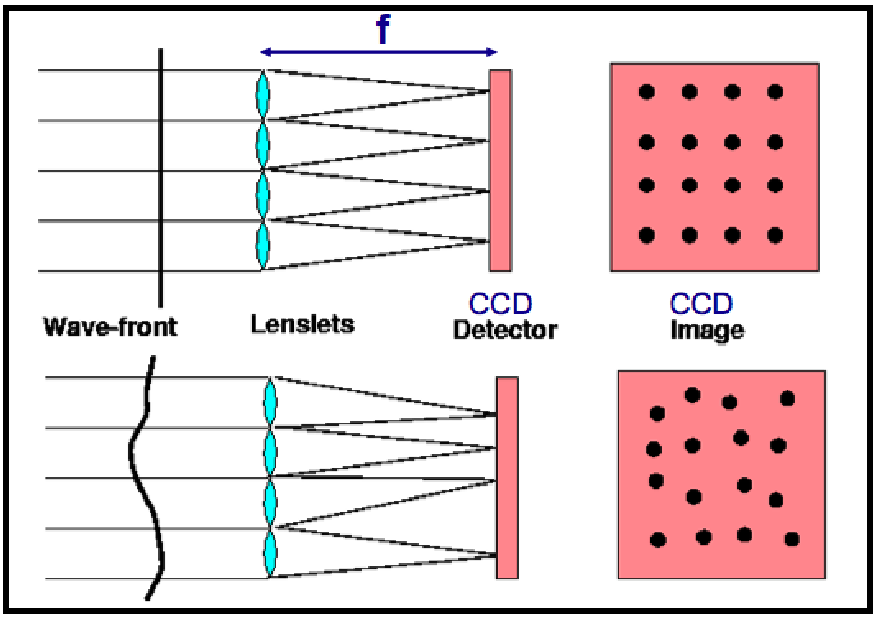

Figure 6 Typical Shack-Hartmann Lenslet Array Wavefront Sensor. Shack-Hartmann WFS illustration courtesy of Center for Adaptive Optics Website.

2. Phase Diversity

The second most common technique of wavefront sensing is Phase Diversity or curvature sensing. Curvature sensing differs from Shack-Hartmann in that it detects changes in the wavefront surface curvature vice slope. The advantage of this is that the curvature of the wavefront can be mapped directly to the surface curvature of the deformable mirror saving valuable computational time. Additionally, where Shack-Hartmann breaks down in the absence of continuous edges, Phase Diversity does not. This allows for wavefront reconstruction across segments of segmented mirror arrays which are becoming in more common use. Finally, Phase Diversity systems have proven particularly useful for optical alignment in AO systems employing mirrors which have capability for corrections of piston. Piston is the movement of the mirror fore-and-aft and such movement causes a detectable change in intensity and beam size. This type of aberration can be corrected by PD sensing but not Shack-Hartmann, due to the inability of a S-H slope sensor to detect this kind of change.

The PD WFS works by looking at the difference in intensity of an image though a known aberration (or amount of defocus) to determine the phase of a wavefront. By evaluating how the unknown aberrated wavefront changes when passing through an aberrator with a known effect, the wavefront can be reconstructed.

A common technique for doing this is to evaluate the wavefront at points equidistant on either side of focus. The intensity of a beam will change from one side of focus to the other unless the wavefront is planar. This difference in intensity is linearly related to the curvature, also known as the Laplacain or 2^{nd} derivative of the wavefront. The image to be resolved is simply the combination of two unknown images; the object image and the aberrations in the image. With only one measurement, the unknowns cannot easily be separated. However, with these two cleverly arranged measurements they can. Given this extra information, an exact solution for both the unknown aberrations and the unknown object, to within the resolving power of the optics is achieved. (Lofdahl, M. G., 1996)

The ability of doing wavefront sensing and image de-convolution based on only two frames greatly reduces the amount of data that needs to be collected. This is particularly important when large detector arrays are used, since the read-out time of current CCD's restricts the number of images which can be read out within a time interval. (Löfdahl, M. G., 1996)

The Phase Diversity system built for this research consists of two cameras arranged equidistant and on either side of focus as shown in Figure 7 If the incoming wavefront is planar, then as mentioned above, all incoming rays meet at the focus and the intensity detected in both planes is equal. If however, the incoming wavefront is aberrated then there will be a difference in intensity such that a bright area would appear on one side of focus and a dimmer spot would appear on the other. By registering the two cameras such that individual pixels can be correlated, this point-wise difference in intensity can be found and the wavefront evaluated.

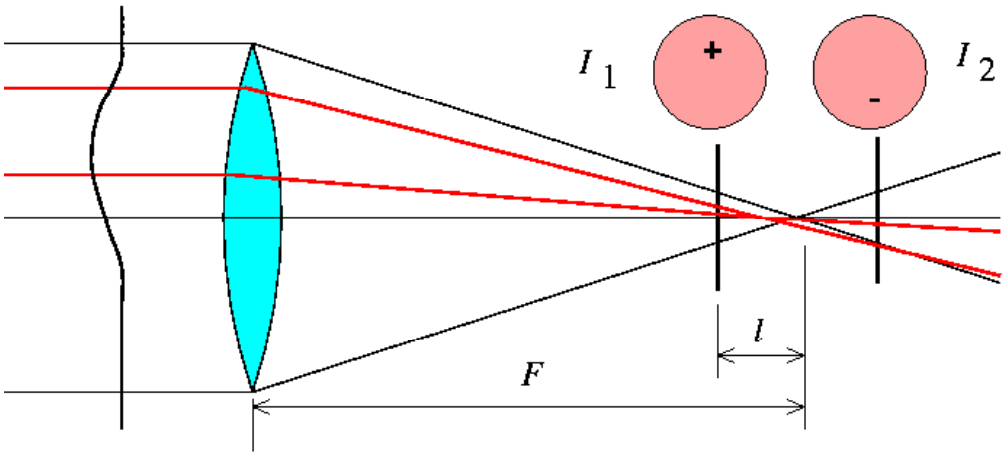

Figure 7 Basic Phase Diversity showing intensity difference between two detector planes equidistant placed either side of focus. Illustration courtesy of Center for Adaptive Optics Website.

C. THE FAMILY OF DEFORMABLE MIRRORS

The attractiveness of a phase diversity system lies in the inherent properties of the bi-morph and micro-machine deformable type mirrors to which it is used. The bulk of this discussion will revolve around these two mirrors. However, since other mirrors will be used in the overall research for which this project is a part, they will be given a cursory review below.

1. The Fast-Steering Mirror or "Tip-Tilt" mirror is the simplest image corrector. It is capable of correcting for movements either onboard the optical platform or the majority of atmospherics by applying 2-dimensional offsets in "tip and tilt." It is used in the SRDC 3 loop AO system discussed in Chapter V and identified in Figure 24

2. Piezoelectric Deformable Mirrors (PDM's) use glass, silicon or fused silica, as a reflective surface depending on application. Unlike MMDM's, they incorporate a 2D array of actuators giving a full push-pull control feature. However, the edges are free and lend to more error there and thus, the PDM's themselves have a 7-15% hysteresis. They are most suitable for fast–feedback control algorithms. This type mirror is again used in the SRDC 3 loop AO system and identified in Figure 24 (OKO, 2006)

3. Segmented Mirrors are typically an array of FSM used in conjunction to create larger than possible apertures for an AO system. There is promising research in the potential for combining tip-tilt correction with MMDM's in a segmented mirror system. This is the technology used in the Keck Observatory and will be used on the Webb Space Telescope, scheduled to replace Hubble in 2011. It is the ultimate intent of the SRDC to replace the current primary deformable mirror in the SRDC's 3-Loop AO system, with a segmented mirror and thus the impetus for this research. One limitation of the Shack-Hartmann WFS is that alone it cannot compensate for wavefront discontinuities across the segment edges of a segmented mirror AO system. However using a phase diversity wavefront sensing technique, the phase information of the wavefront can be maintained and the wavefront reconstructed. The final objective of the SRDC will be to combine the capabilities of a phase diversity WFS with a Shack-Hartmann to control this improved segmented primary mirror where individual segments have the properties of an MMDM or Bi-morph mirror.

4. Micro-machined Membrane Deformable Mirror (MMDM) is a thin membrane mirror with fixed edges. Its nominal shape is spherical due to its edge only actuators having electrostatic push-only application. It is important to note that the un-powered (voltage=0) position of the MMDM is relatively flat with the membrane resting against its back plate. This requires that the MMDM be powered to a pre-determined neutral bias position such that corrective travel is available for the actuators in either fore or aft positions. This "neutral bias position" is shown in the next section to be roughly 180 volts for all actuators and gives the mirror its initial reference spherical shape.

As previously mentioned, the advantage of the phase diversity system is that it takes advantage of the analog physical property of the MMDM to first order approximations such that the wavefront itself can be correlated directly to the face-sheet of the MMDM or Bi-morph mirror and conjugational computation is simplified. By manipulating the shape (curvature) of the mirror surface the curvature of the wavefront can be conjugated for wavefront reconstruction by one-to-one mapping (curvature of the wavefront with curvature of the mirror surface).

D. THE PHYSICS OF THE CONCEPT

The mathematical properties of the MMDM and Bi-morph mirror have been studied at length and are summarized below.

In establishing the relationship between wavefront surface ϕ, wavefront curvature $\nabla^2\phi$, Intensity I, and Actuator Voltage V, we develop the association between the wavefront, PD wavefront sensor, and the deformable mirror with the plainest objective of relating observed Intensity difference with actuator Voltages necessary for mirror conjugation.

The Roddier brothers in their paper "Curvature Sensing and compensation; a new concept in Adaptive Optics" surmised that the local wavefront curvature or the Laplacian of the surface is defined:

$$\nabla^2 f(x,y) = \frac{\partial^2 f(x,y)}{\partial x^2} + \frac{\partial^2 f(x,y)}{\partial y^2} \tag{2.12}$$

A point-by-point subtraction of the illumination in each image is approximately equal to the wavefront curvature term:

$$\frac{I_{p1} - I_{p2}}{z_1 - z_2} \approx \frac{\partial I}{\partial z} \tag{2.13}$$

with z denoting the distance from the focal point of each image plane. Finally, where k is the wave number, the wavefront curvature is related to the axial intensity derivative through the intensity transport equation:

$$-\frac{k}{I}\frac{\partial I}{\partial z} = \nabla^2\phi \tag{2.14}$$

Thus the change in intensity is proportional to the curvature of the wavefront. (CFAO, 2007). Now turning to the formulation of the bimorph mirror, Burley, Stilburn, and Walker showed that the curvature of the MMDM and bimorph mirror is governed by the Poisson equation

$$\nabla^2 Z = cV^2 \tag{2.15}$$

where c is a constant related to the tension in the membrane surface, the size of the actuators, the distance between the actuators, and the permittivity of free space. Additionally since we describe in the introductory of this work that the nature of the relationship between the wavefront and a mirror surface curvature is simply:

$$\nabla^2 Z = 2\nabla^2 \phi \tag{2.16}$$

we have thus:

$$\nabla^2 \phi = CV^2 \tag{2.17}$$

Since the mirror is electrostatic and has response to push only and it rests against its back-plate at V=0, it must be electrically biased to its neutral position such that travel in both fore and aft directions can be achieved and wavefront curvature can be corrected. This bias position is governed by the voltage–mirror response formula given in the OKO technical manual for the specific mirror we are using. The formula is:

$$V \propto CS = 255\sqrt{.5(CB+1)} \tag{2.18}$$

where CB is the control byte sent to the mirror using the "Front Surfer" program with range or -1 to 1, and CS is the control signal to the mirror with a range of 0-255 (OKO 2006). In "Front Surfer" CB=0 is the mirror's neutrally biased position and corresponds to its position with maximum available range of throw, in either direction. Since the Matlab coding for this research was written to use CS or Voltages normalized to range from 0-255, this neutral bias position is achieved by setting all actuator values to 180.31 where CB=0. This 180.31 will serve as our V_0 (initial voltage) from whence a ΔV can be applied. For this paper the terms Voltage and Control Signal are interchangeable as the CS is only a scaled voltage.

Now continuing from above, since

$$V = V_0 + \Delta V \tag{2.19}$$

and from 2.17 $\nabla^2 \phi = CV^2$ with the higher order ΔV^2 ignored after computing V^2 we have,

$$\nabla^2 \phi = 2CV_0 \Delta V + CV_0^{\,2} \tag{2.20}$$

(Burley, Stilburn, and Walker, 1998).

Thus we have shown that the mirror curvature is a linear function of ΔV and since the conjugated mirror can mimic the wavefront surface by design, we show that the change in intensity is linearly related to the change in voltage ΔV by:

$$-\frac{k}{I}\frac{\partial I}{\partial z} = 2CV_0\Delta V + CV_0^{\,2} \tag{2.21}$$

Now assuming that a statistically significant but small ΔV can be applied to any actuator such that its influence can be isolated from the areas of influence under its adjacent actuators, we can determine the value of C. Since this value comes from the electrostatic and tension properties of the mirror, it should be constant regardless of which actuator is used. (Roddier C., Roddier F., 1988)

Therefore in the simplest of terms, for all actuators the tension constant can be found though:

$$\Delta\bar{I} \,/\, \Delta V = c \tag{2.22}$$

where $\Delta\bar{I}$ is the average change in intensity observed in the influence area for a given ΔV.

Thus with our constant c in hand, we only have to relate any regionally observed change in intensity multiplied by a constant to yield the voltage array necessary to conjugate the mirror. This conjugation gets further refined as an iterative closed loop process as the voltage applied moves the mirror to conjugation and a net intensity matrix is formed. This new matrix is then re-evaluated and the process continues limited only by processing speed.

The key to this technique is the registration of the mirror and its actuators. Once we have the association between individual actuator location and the influence of a voltage applied, we can establish the full registration in the form of a vector relation.

$$\frac{1}{c}\left[\Delta\bar{I}\right] = \left[\Delta V\right] \quad \frac{1}{c}\left[\Delta\bar{I}\right] = \left[\Delta V\right] \tag{2.23}$$

Where the vectors

$\left[\Delta\bar{I}\right] and \left[\Delta V\right]$

consist of n elements equal to the number of mirror actuators. In the case of this research and in the interests of simplicity for proof of concept, only 18 actuators of a 59 actuator mirror were used.

THIS PAGE INTENTIONALLY LEFT BLANK

III. PHASE DIVERSITY WAVEFRONT SENSING TEST BED

A. COMPONENTS:

The Phase diversity table was set up using Edmund and Newport optics with a limit of diffraction rating of .25 λ. The primary functional components of the PD table are:

Laser
OKO 59 actuator MMDM
2 Photon Focus CMOS Cameras
Shack-Hartmann WFS
2 Computers (one to drive the MMDM and the other to read the PD data)
The "Front Surfer" software program

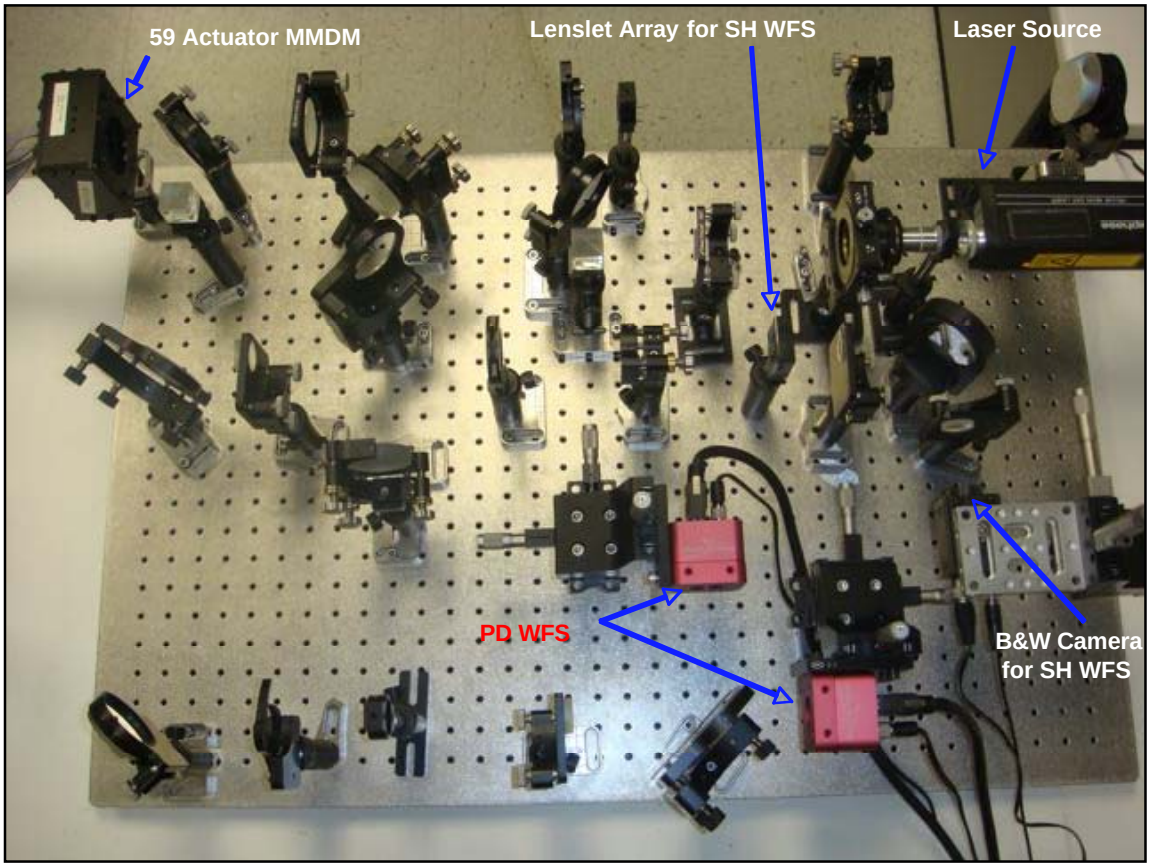

Figure 8 The layout of the Phase Diversity Test Bed.

1. Laser

Though the PD system was initially established with a HeNe laser, the unit was determined to have polarization issues which proved incompatible with the experiment. In the final stages of work, a 532 nm green laser was placed in the system which proved more conducive to the PD system.

2. Micro-machined Membrane Deformable Mirror (MMDM)

The 59 Actuator OKO MMDM was loaned to NPS from the Adaptive Optics researchers at the Naval Research Laboratory in Albuquerque NM. As the name implies the mirror has 59 actuators and they are arranged numerically in order and in concentric circles with actuator number one in the center followed with the remainder arranged over five rings. Figure 9 gives a depiction of the mirror actuators. As stated above, in the interests of simplicity and that necessary only for proof of concept, it was deemed adequate that the first three rings of actuators (numbers 1-18) would be used for the work detailed in this paper.

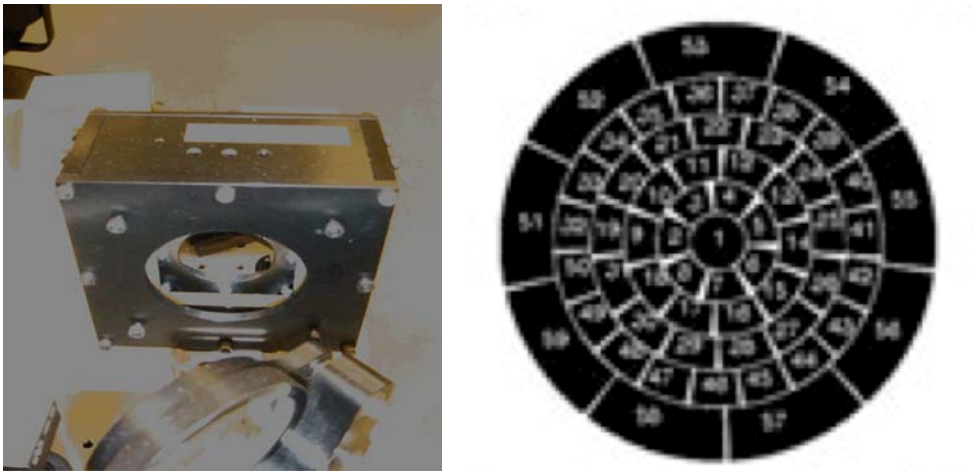

Figure 9 The OKO 59 actuator mirror (photo left and actuator arrangement right) (OKO, 2006).

3. Shack-Hartmann Wavefront Sensor

For this research, an expensive Shack-Hartmann was not available. However, using a black-and-white CCD camera and an inexpensive plastic lenslet array, one was made which would suffice for this research. The idea was, that using the off the shelf "Front Surfer" wavefront analysis program, a known wavefront could be input to the Phase Diversity WFS, detected and computationally conjugated out with the MMDM which was controlled by Matlab algorithm using the intensity data collected by the PD WFS.

4. Phase Diversity Sensor

The PD sensor was made using two Photon Focus 1024x1024 pixel CMOS cameras set to 20 Hz, purchased specifically for this work. They were arranged 20 mm equidistant on either side of focus of a 200mm focal length with the intensity difference image divided by a 50-50 flat plate beam splitter. The 20 mm equidistance from focus was determined be the maximum distance for desired sensitivity results of .25 λ using the Zemax optical modeling program.

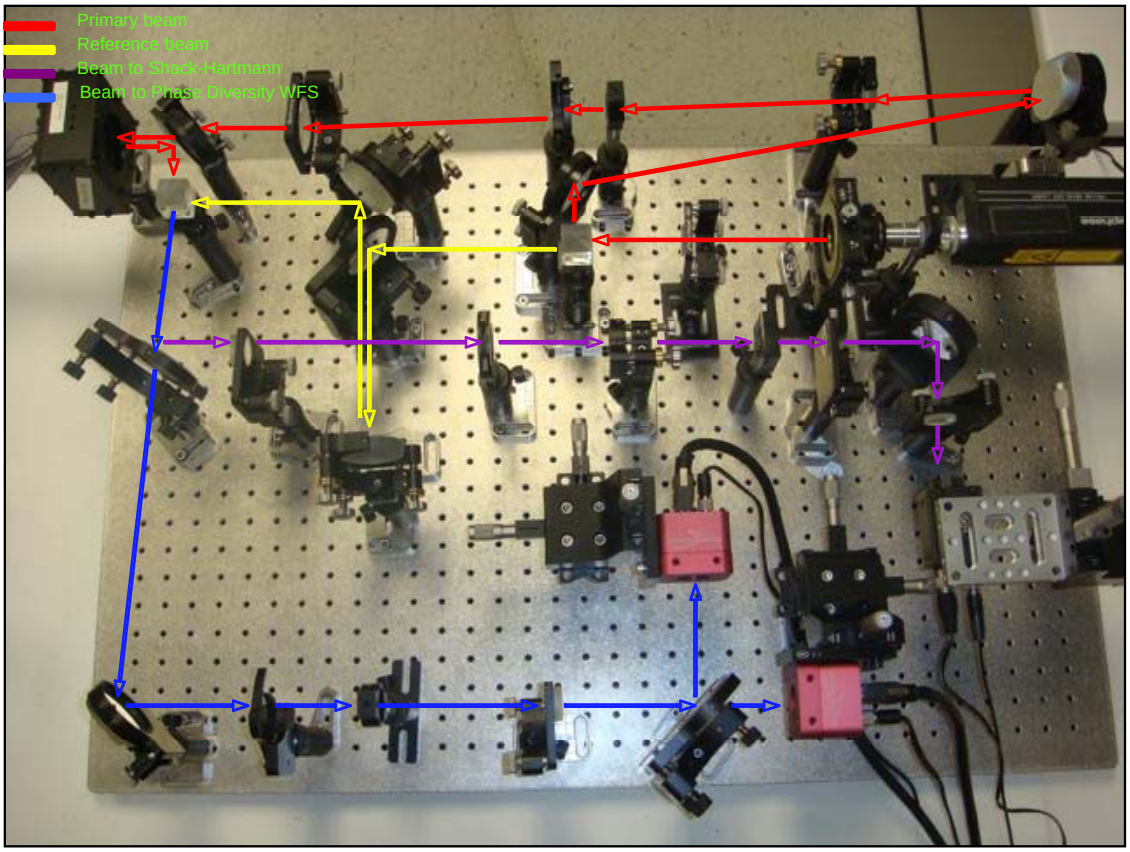

Figure 10 Beam path for the Phase Diversity Test Bed.

5. Computer Feedback Control

Due to the number of PCI slots required to run each system, two computers were required to close the loop between the PD WFS and the MMDM. The Photon Focus cameras required 1 PCI slot each and the 59 actuator MMDM required three PCI slots. Thus, one computer housed the MMDM controls and the "Front Surfer" program while the second housed the frame grabbers and control cards for the 2 Photon Focus cameras.

Matlab algorithms were written such that control of the MMDM was available via both "Front Surfer" and directly from Matlab script for the MMDM. The Photon Focus (PD WFS) control computer was used to develop the Matlab routines necessary to read the data from the PD system. This PD information (intensity difference data) was passed in closed loop routine to the MMDM control computer via Ethernet and the mirror

controlled. This allowed for the "Front Surfer" program to be used in evaluating the performance of the PD WFS Matlab algorithms.

6. The Front Surfer Program

Much of the current research undertaken at the NPS Spacecraft Research and Development Laboratory uses the off-the-shelf "Front Surfer" program for wavefront analysis and deformable mirror control. This provides an excellent resource for results comparison such that the AO test beds can be optimized and refinement of mirror control MATLAB algorithms can be made.

The "Front Surfer" program published by OKO Technologies reconstructs the wavefront from a Shack-Hartmann wavefront sensor. (Note: it is not capable of using data from a Phase Diversity AO system). It produces data in the form of mirror individual actuator throw measurements, Zernike polynomial interpretation, interferogram contour map display, point spread intensity display, and wavefront surface representation. In quantifiable terms, "Front Surfer" calculates the peak-to-valley measurement of the wavefront such that it can be compared to the diffraction limits of the optical system in use. The SRDC uses optics rated for .25λ and thus calculated resolutions less that .25λ are consider diffraction limited. Figure 11 gives an example of the "Front Surfer" program output display showing, lenslet array detection, wavefront surface depiction, far field intensity display showing the desired airy disk of good resolution, and a clean contour map interferogram showing the majority of aberration.

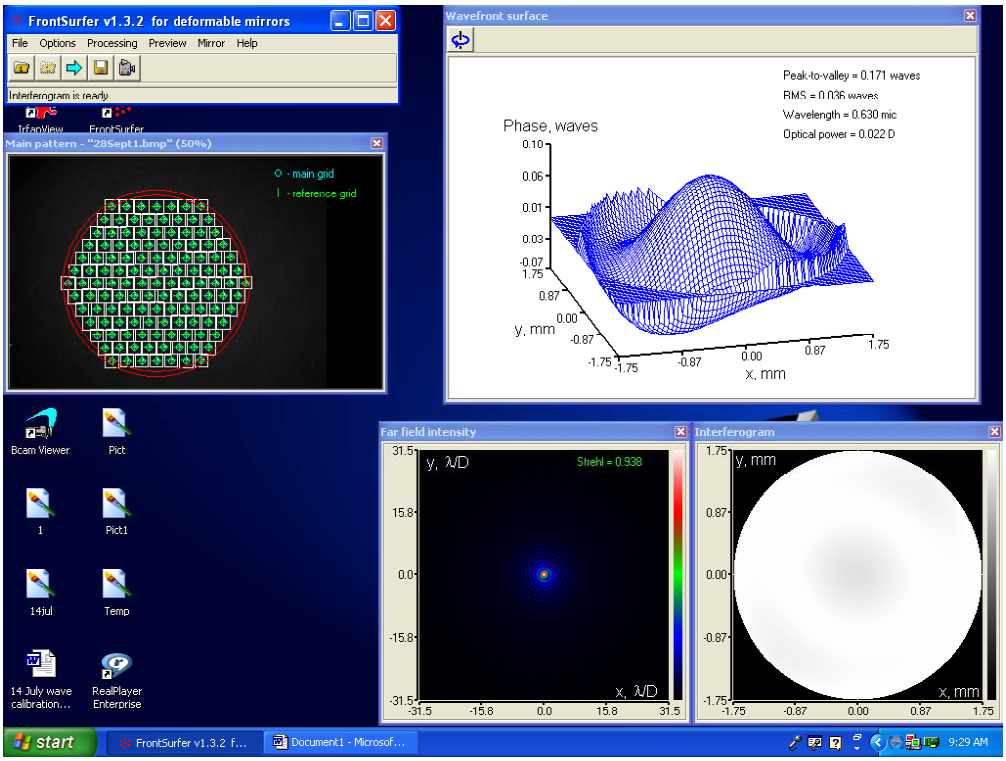

Figure 11 Typical example of "Front Surfer" program output showing, wavefront resolved to .171 waves, less than the diffraction limits desired of an optimized AO system of .25 λ.

The "Front Surfer" output shows the detected lenslet array on the far left followed by a surface depiction of the wavefront with a quantitative RMS and wavelength "peak-to-valley" measurements. It should be noted here that the scale of the wavefront depiction always changes and thus must be closely examined against the RMS and wavelength peak-to-valley to discern the fidelity of the data. Finally, in the lower sections of the output are the "Far Field Intensity" along with a contour map "Interferogram" of the resolved beam.

If the wavefront has been properly resolved by the system it should closely resemble the initial reference which the MMDM wishes to reproduce. Ideally, this reference and resolved (corrected beam image wavefront) would be represented by an

airy disk point in the Far Field Intensity display, a white Interferogram depicting no contours and a Peak-to-Valley resolution less than .25λ. Figure 12 shows typical output depictions with quantifiable data.

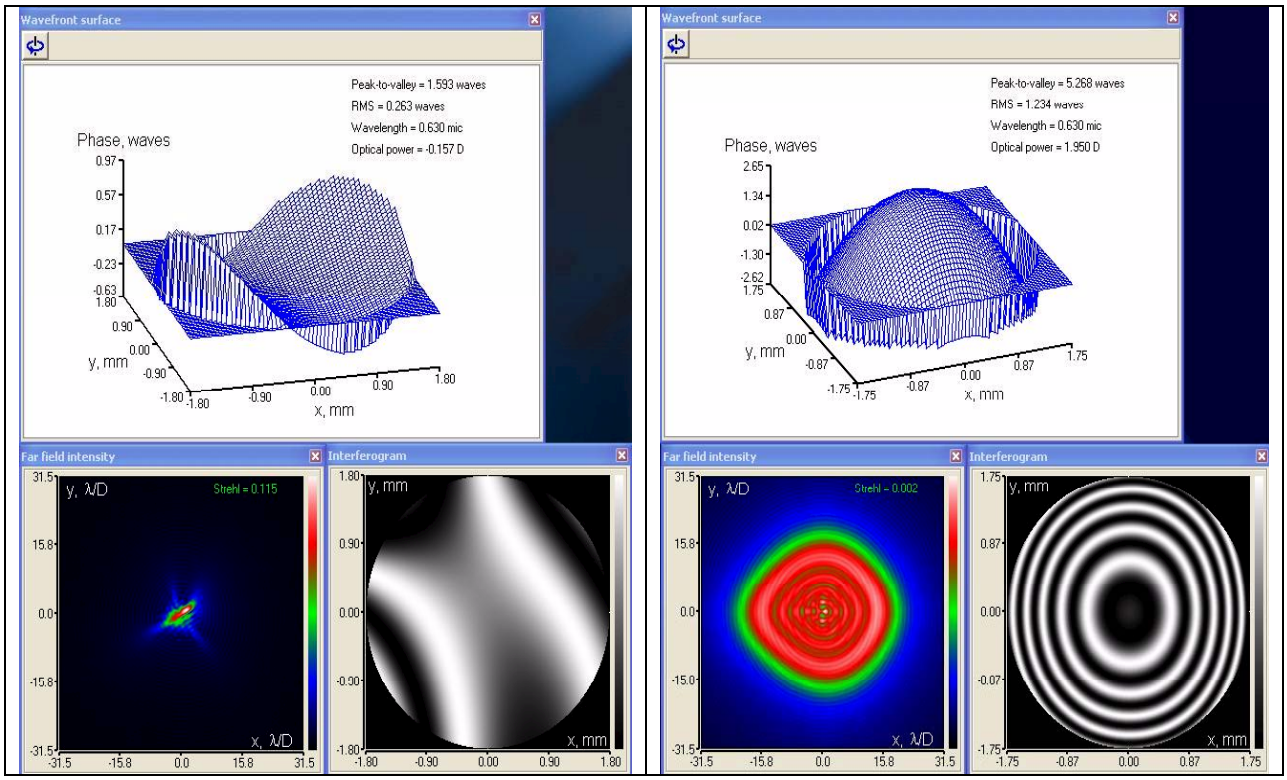

Figure 12 Typical "Front Surfer" output depictions showing far field intensity, contour map and wavefront peak-to-valley data differences.

B. ZEMAX MODEL:

In order to predict the resolution capability of the phase diversity system, a model of the optical system was generated in Zemax. Zemax is the industry standard modeling program used for optical engineering. The objective of the model was to establish that resolution close to the limits of diffraction could be achieved by the PD system.

By evaluating two modeled images on either side of focus, the difference in intensity was examined to determine if the system would be sensitive enough to detect an intensity difference caused by aberrations. In Figure 13, we see the modeled interferogram on either side of focus at 20 mm for a 200 FL lens. Figure 14 shows the

modeled difference between the two images with .25 waves of astigmatism induced into the system once the reference background has been subtracted out. Notice the darkening of the fringes on the sides while on the top and bottom are brighter. This noticeable asymmetry established the sensitivity of the system to within .25 λ.

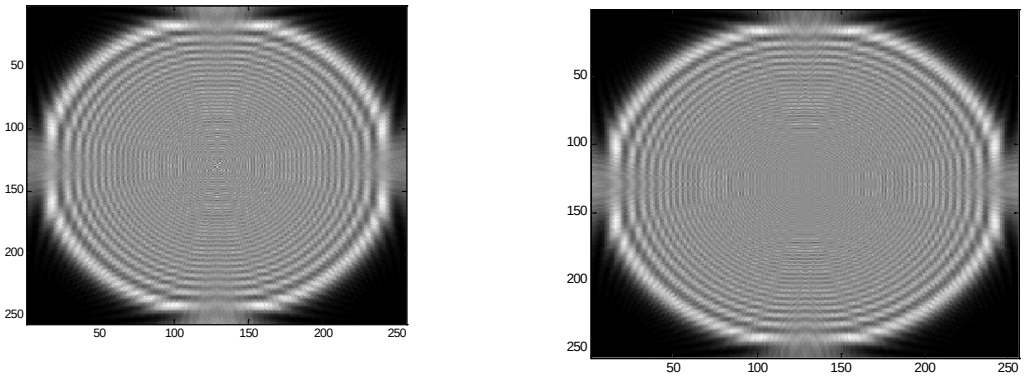

Figure 13 Zemax modeled image 20 mm in front (left) and behind (right) of 200 mm FL lens.

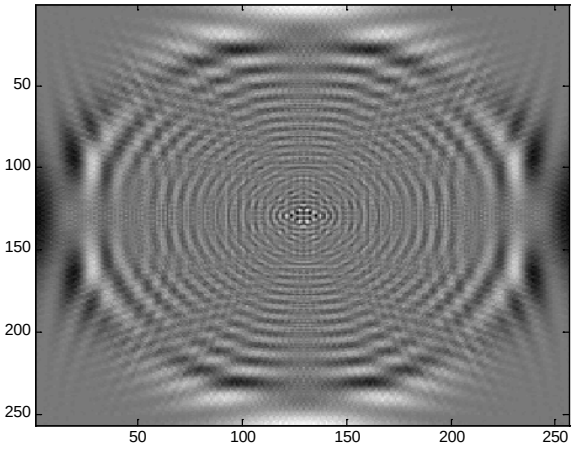

Figure 14 Zemax modeled intensity difference (with background subtracted) of two images in Figure 13 The bright fringes on top and bottom compared to dark fringes on the sides denotes noticeable astigmatism and demonstrates the fidelity of the PD optical system to detect aberrations less than .25λ.

IV. PHASE DIVERSITY EXPERIMENTS

A. EXPERIMENTAL SETUP

The vast majority of the work conducted for this research over the last two years has been in the background of the optical science necessary to make a phase diversity system work. In looking at the diagrams and photographs of the current Phase Diversity table one will see a very complicated system of lenses, beam splitters, mirrors, spatial filters and more. Every intricacy of the table's design had to be researched and planned, and the final product shown here is only the last of many intermediate designs. Mastery of the sciences of physical optics and optical engineering were critical elements necessary in building the foundation from which this research could start and shall be continued by the SRDC. However, since review of this foundational background is not critical for the specifics of this research, we will skip to the intricacies unique to this work. Finally in the following section many of the figures contain four individual pictures. They are of the two PD cameras (top) while the bottom two images depict their intensity difference one subtracted from the other and vice versa. This is essentially a superposition of the two images.

1. Optical Alignment of the System

Proper alignment of the system was critical for the successful conduct of the research. Every single optical component had to be placed as precisely as possible such that the beam incidence was perfectly normal, reflected properly, and the optical piece was placed at the exact distance necessary for proper focus or columniation as required. Additionally, the test bed was prone to the effects of the slightest environmental changes, from temperature changes to building vibrations. This resulted in time consuming, daily alignment adjustments.

The alignment of the beam was evaluated through the system by a reference path denoted in yellow in Figure 10 This reference was imaged on the two Photon Focus cameras. Under ideal conditions the reference beam image would be a perfect circle with the diffraction pattern depicted in the Zemax model Figure 13. Figure 15 (Left) shows

this reference pattern directly from the PD table. Note the slight elongation of the beam images denoting that residual astigmatism in the system could only be minimized.

2. Neutral Biasing the MMDM

As mentioned before it was critical to use the MMDM in its neutral bias position (all actuators placed at 180.31 volts) to give corrective throw fore-and-aft for conjugation of the mirror. This had a tendency to introduce additional astigmatism into the system due to the curved shape of the mirror while in this biased position. This astigmatism is seen in Figure 15 (Right) where one camera depiction in the upper left is oblong side-to-side while the second camera is oblong top-to-bottom. This astigmatism could be partially corrected for through background subtraction and further compensated during correction or conjugation of the MMDM.

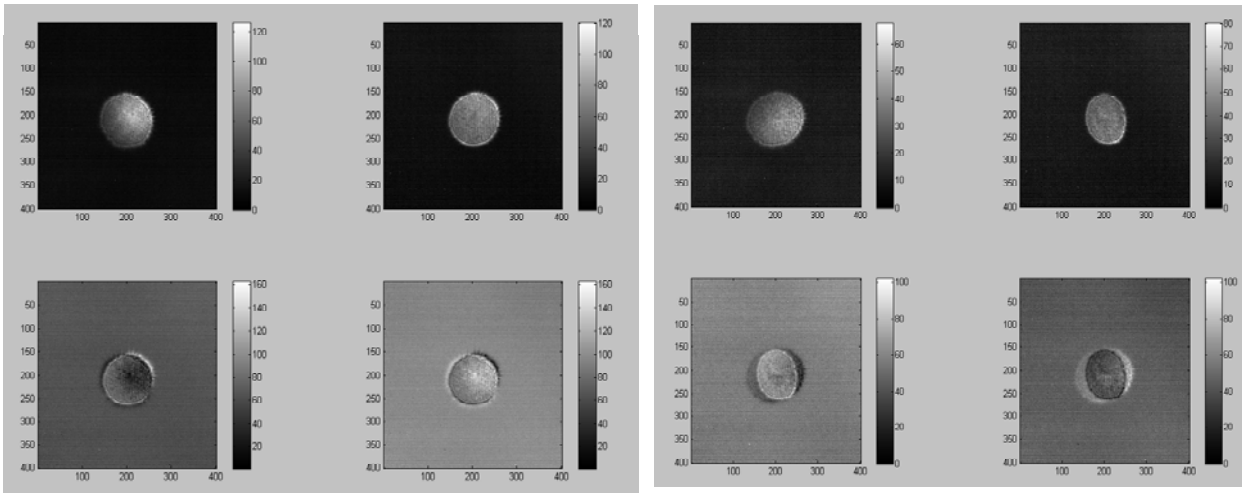

Figure 15 (Left) showing the reference unaberrated beam detected by the PD system with the intensity difference of the two cameras in the bottom two images. (Right) showing the PD image of the MMDM in its neutral bias position. Note the astigmatism caused by the fact that in its neutral position, the MMDM is not flat but in fact somewhat spherical.

3. Camera Imaging

The two cameras were controlled via Matlab script with one camera serving as a master working in one iteration of Matlab, while the second camera operated as the slave,

using a second Matlab iteration. The camera's intensity matrix output could then be analyzed in Matlab and using the imaging features of the program, visual representations could be evaluated. Figure 15 and Figure 16 show such an output.

The cameras were set up and the data represented pixel by pixel in a 1024x1024 intensity matrix. The two intensity matrices (one from each camera) were then subtracted to give an intensity difference matrix. This intensity difference matrix was then further paired down to a 400x400 matrix in Matlab by eliminating the vast majority of unused camera pixels and thus rendering a much more computationally friendly, "intensity difference matrix." It is from this paired-down intensity difference matrix that manipulations to the MMDM were made and changes in the intensity difference explored. Figure 16 (Left) shows actuator number one being moved a small ΔV=10 volts, such that the intensity difference is accentuated. In fact, the actuation is so small that it is barely (if at all) noticeable on each of the individual cameras. However, in the bottom two images of the same left figure where the "difference" in intensity is imaged, the actuation stands out prominently. Figure 16 (Right) shows the same actuation but at a more prominent $\Delta V = 75$ volts.

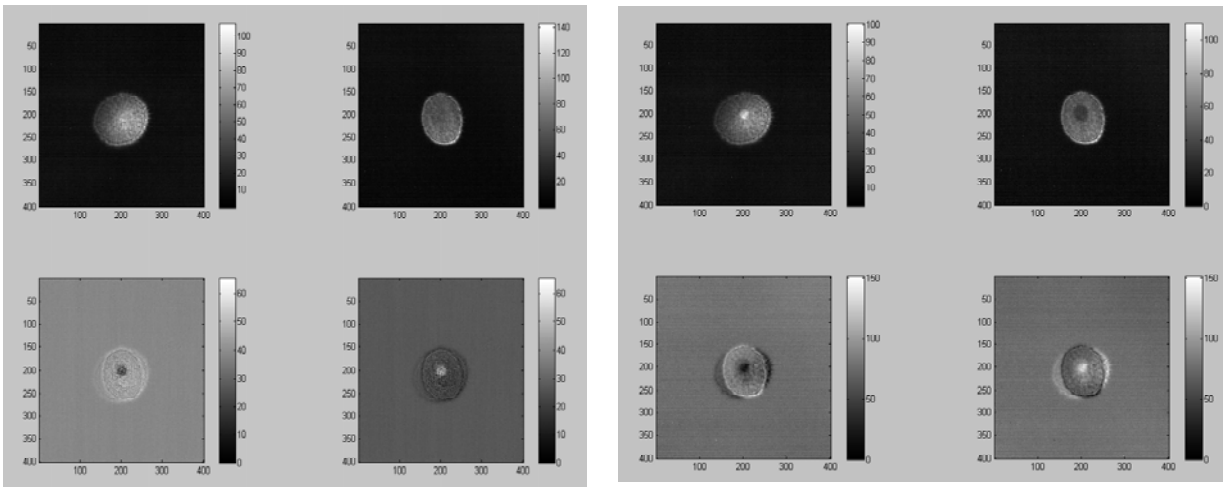

Figure 16 The MMDM with actuator one actuated by 10volts on the left and 75 volts on the right. Notice the intensity difference stands out prominently on the left (bottom) while the raw intensity (top) barely hints that an actuator has moved.

4. Matlab Control of the PD System

Each camera's array of 1024x1024 pixels served as intensity detectors and rendered a scaled intensity value from 0 to 255 depending on the level of light intensity detected by each pixel. When necessary, neutral density filters were used to reduce beam intensity reaching the camera CMOS detectors such that they were not saturated (all intensity values less than 255).

Intensity management was a critical factor in the accurate evaluation of the PD system. It was very important that the total power intensity arriving at one camera did not significantly differ significantly from that of the other. Though the beam was being split by a 50-50 flat plate beam splitter, there was still an observed difference in total intensity reaching the two cameras. One camera was detecting 7% more power. To remedy this, the total intensity values were normalized to each other such that under the most ideal circumstances of a planar wavefront, the beam intensity observed at any one camera pixel would have the same value at the corresponding pixel on the other camera.

5. Removing Hot Pixels

Next the issue of hot pixels had to be addressed. Due to the large size of the matrices it was necessary to systematically eliminate those few pixels which were not functioning properly such that the computational algorithms would not use the bad data. Simply, there were some pixels whose value indicated that they were always saturated regardless of intensity. These pixels were eliminated by dark-covering the cameras and for any pixel in the resulting intensity matrix which registered an intensity value above a certain point, that pixel's value was set to zero with an if-then loop, while all others were set to a value of one. This resulting "hot-pixel matrix" comprised almost entirely of ones save those few zeroed-out hot pixels was then multiplied by the original intensity matrix. This resulted in the elimination of all hot pixel data from the analysis which otherwise would skew the data.

6. Background Subtraction

Due to the fact that there will always be inherent astigmatism, diffraction and other minor aberrations of the intensity images, it was necessary to minimize these constant imperfections from the optical system through a process of background subtraction. This was done by imaging the intensity difference of the two cameras while viewing a planar reference wavefront of the neutrally biased mirror. Ideally, this image would show nothing discernable but Figure 17 (Left) gives the definite hint of this background (reference) image; which if not removed would contribute unwanted noise to the data. Figure 17 (Right) shows the intensity difference of the two cameras with the background (Left) subtracted and data smoothed while giving actuator number one of the MMDM a slight 10 volt actuation.

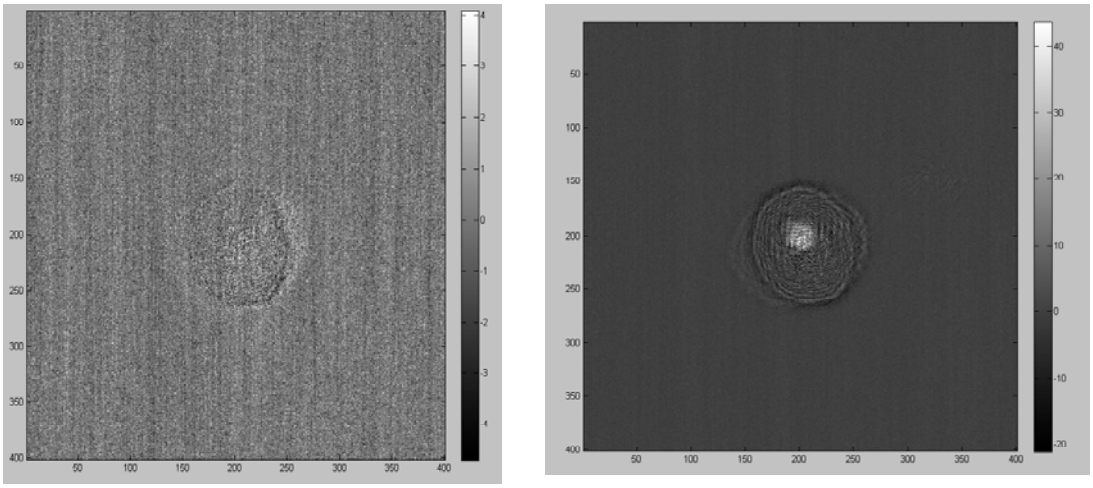

Figure 17 Left shows a typical background reference image (no actuation) and simply registering the fundamental intensity difference between the PD cameras. This was always subtracted out for the reduction of noise in the system. Right shows a typical intensity difference image (actuator #1 at ΔV =10 volts) with the reference background image subtracted out.

7. Smoothing the Data

Close examination of the data showed that the intensity in any one area of influence had a tendency to vary a widely from individual pixel to the next adjacent pixel. This is most likely due (at least in part) to the expected diffraction fringes predicted in Zemax. In order to compensate for this such that a good average difference in intensity for the area of influence could be determined, a convolution smoothing algorithm was run over the intensity difference matrix. Additionally, a noise floor was established such that any measured intensity difference outside significant values was discounted.

8. Registering the Images

Another challenge in evaluating data derived from two cameras lay in the registration of the cameras and their individual pixels. It was critical when looking at identical pictures, or pictures in which we wished to minimize the difference, that any individual pixel could be associated with its counterpart on the other camera. This "registration" allowed for the correlation of the intensity detected at one pixel, to that of the other. To accomplish a crude registration, a cross-hair fiducial was used to obtain rough alignment of the two cameras. A more refined registration was accomplished by looking at the influence of each individual MMDM actuator to ensure that any observed intensity difference in one image would be superimposed concentrically over the intensity change in the other camera image. Figure 17 (Right) shows actuator number one being actuated alone while Figure 18 shows actuation of actuators one and nine together.

9. Establishing the Tension Constant

The tension constant was established by taking an average difference in the smoothed intensity data observed while actuating a single actuator, and dividing it by the small ΔV which caused the observed influence (as outlined in section IID). This constant, as the name implies, is a function of the tension in the membrane. However, it is also a function of the area of the individual actuator pad, the separation between pads, and the permittivity of free space. The tension constant for this particular MMDM was

determined experimentally to lie between -1.5 and -8.8 with an average of -3.5. The -3.5 value was used for the remainder of the project. Any error in this value would be compensated for in setting the gain of the control algorithm where the time for convergence of the control law was effected by the accuracy of this constant.

10. Centroiding the Actuators

With proper registration of the individual actuators, it was now possible to establish the centroids of influence from any observed actuation. The actuation centroid locations were critical for correlating average differential intensity areas with the appropriate actuator to be driven in order to minimize this computed difference. To accomplish this, each of the 18 actuators used in this project were individually actuated and their centroids annotated in a call back Matlab file. From these centroids, a window, whose size was optimized at 20x20 pixels by evaluating the influence distance between actuators as imaged by the PD cameras, was established around the centroid and the average intensity difference was measured during each iteration of the PD control loop. For full MMDM operation, 59 centroided windows would map to 59 ΔV's, one for each actuator, and as the MMDM began its control loop iterative process, the intensity difference in each area of influence should approach its minimum. Table 1. shows the centroid locations for each of the 18 actuators used in this research.

Table 1. The actuator centroid data, determined by individual influence of each actuator 1-18 by ΔV = 10 volts. The numbers represent the pixel location of the center of actuation from which a window was established for which the average intensity was used.

Actuator	Pixel Centroid	
1	202	200
2	202	222
3	215	211
4	218	196
5	210	182
6	194	182
7	182	197
8	186	215
9	200	236
10	218	230
11	231	210
12	232	188
13	223	173
14	199	169
15	180	175
16	169	192
17	171	212
18	184	234

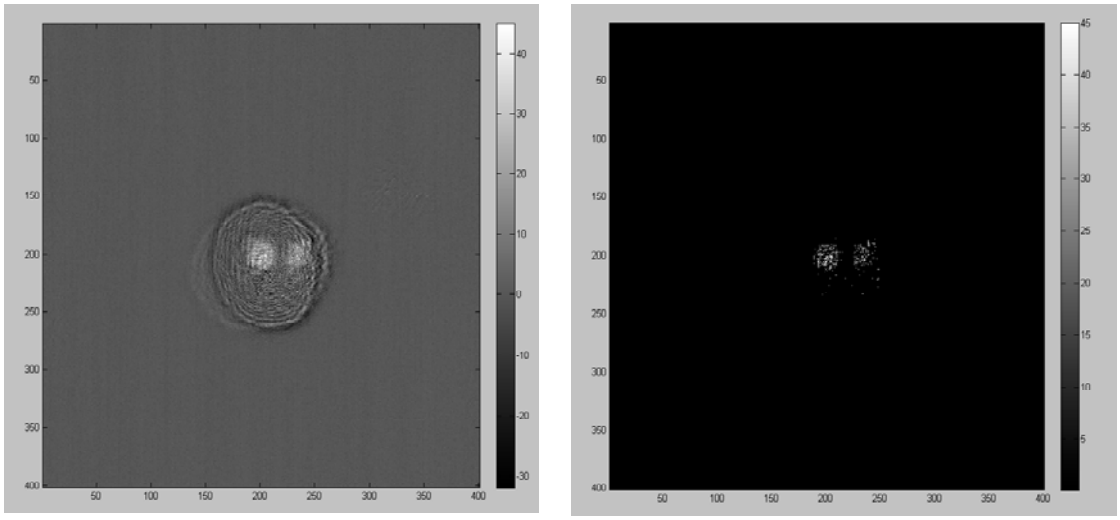

Figure 18 Left shows the actuation of actuators #1 and 9 simultaneously by a small ΔV =10 volts while the right shows the same image with the noise threshold set to a level which helped in highlighting the centroids of actuation based on the areas of largest intensity difference. Note: centroids were determined though individual actuations of actuators 1-18.

11. MMDM Control

Finally the MMDM was controlled by a basic control loop $V_{new} = V_{old} - K * \Delta V$ where ΔV is computed from equation (2.22) and the intensity difference in each influence area of actuation, 18 in this case, was determined in the Matlab script for the PD system and the mirror conjugated iteratively to minimize the sensed intensity difference. Numerous K values were used with .3 converging quickly and values above .5 going unstable.

B. EXPERIMENTS AND RESULTS:

Two separate types of experiments were conducted to prove the concept and the functionality of the designed phase diversity system. The intent of each was to establish the ability of the PD system to act as a wavefront sensor using Matlab algorithms to control the MMDM. The system was designed to give full readouts of voltages applied to individual actuators, and using the comparator Shack-Hartmann WFS, verify the results with the "Front Surfer" program.

1. Experiment One

Correcting for an Aberrated Wavefront Induced by the MMDM

The simplest experiment used to prove the concept was done by using the MMDM as its own aberrator, and then using the PD system and control algorithms, to correct the mirror back to its neutrally biased position of V=180.31. Simply, with the MMDM in its neutrally biased position, a reference was established in "Front Surfer." The quality of this reference was quantified by self-referencing it and verifying that any observed differences lay within the limits of diffraction of the system. Typical self-referencing results are depicted on the left of Figure 19 The mirror was then manually manipulated to give an extremely distorted wavefront output. The results of this deliberate manipulation are shown on the right in Figure 19

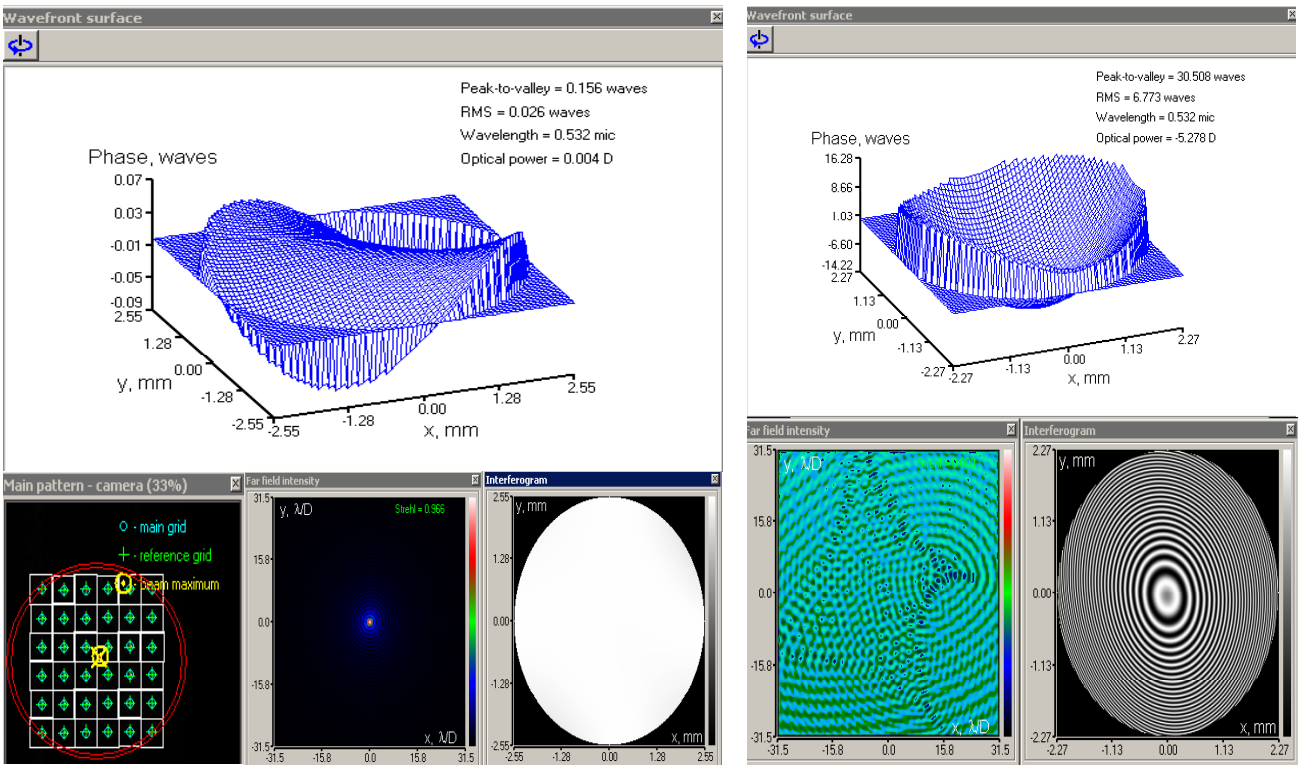

Figure 19 Reference image (Left) established by comparing the difference between two wavefronts taken in close succession and without making any changes to the optical system including the actuators of the MMDM. This is known as self-referencing. Right shows a fully aberrated wavefront, in this case generated through manual manipulation of individual MMDM actuators.

Finally, the system was run from this manually aberrated state and the intensity difference minimization feedback loop from the PD system was executed driving the mirror back towards its neutrally biased reference state of each actuator voltage of approximately 180. This procedure gave excellent results for wildly aberrated wavefronts, but worked entirely inside the dynamic range of the MMDM. Regardless, the value of this particular experiment lies in the fact that such significant corrections could be made to the wavefront (30 waves corrected to .3 waves) in spite of the fact that the full correction capability of the MMDM was not being utilized (only 3 of 6 rings of actuators utilized).

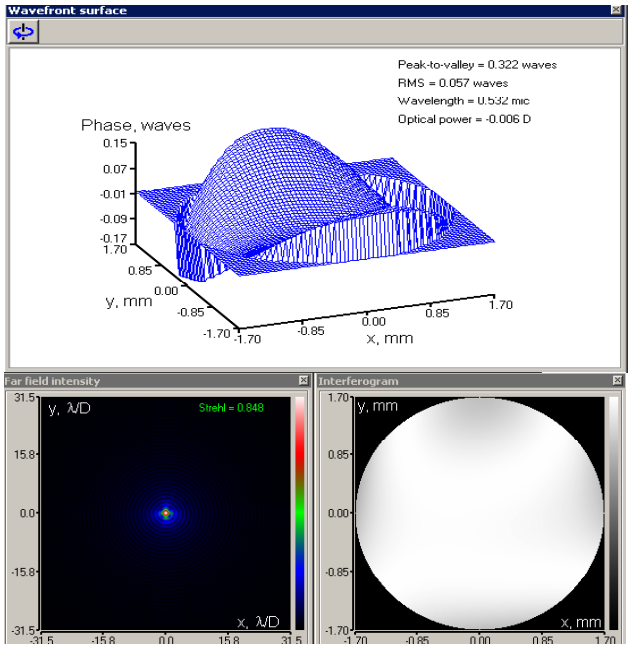

Actuator	Voltages
1	180.4467
2	180.6008
3	180.7724
4	180.9722
5	180.2520
6	180.5782
7	180.5968
8	180.7121
9	180.7571
10	180.9835
11	181.0372
12	180.8679
13	181.0901
14	180.9619
15	180.8320
16	180.4348
17	180.8453
18	180.8850

Figure 20 Corrected wavefront (Left) and final actuator voltages (right) showing 100 times improvement over the original aberration depicted on the right of Figure 19 All actuators driven by the PD WFS back to neutral bias V=180.

During this experiment, numerous control gains were used and though an optimization study was not undertaken, a control gain of .3 worked well. Under these conditions, the control loop ran at 20 iterations per second and Table 2. gives individual actuator values at different points of the closed loop iterative process. This experiment was run numerous times with similar results each time. Typically the system was requiring about 3000 actuations or 150 seconds to stabilize near the neutral bias position of V approximately 180 volts.

Table 2. Individual actuator voltage values after the annotated number of control loop iterations with actuators running at approximately 20 iterations per second.

Actuator Voltages				
Actuator #	10 Actuations	100 Actuations	1000 Actuations	5000 Actuations
1	5.2422	198.9014	179.9660	180.1263
2	4.5054	148.2426	221.4994	180.9212
3	4.0014	126.5450	205.3759	180.6004
4	3.3402	116.7978	182.6091	180.6047
5	2.9142	110.9571	180.3662	180.4802
6	2.6166	100.7768	180.1600	179.9323
7	2.3626	91.0052	191.5349	180.0775
8	3.4356	130.8463	221.7325	180.7440
9	0.5872	47.1431	180.0749	180.0516
10	0.4378	52.7212	180.1137	180.8407
11	0.3277	41.4657	179.1054	180.2002
12	0.9445	52.4089	179.8017	179.9476
13	1.2453	55.8422	180.2689	180.0423
14	1.6936	66.2700	180.1470	180.1273
15	0.7150	29.7258	180.8331	179.9790
16	0.3103	10.9094	178.9915	179.8827
17	0.3550	16.8031	180.4633	180.6826
18	0.0425	21.6902	179.9806	180.0244

2. Experiment Two

Correcting for an Aberrated Wavefront Incident on the MMDM

The second experimental approach was designed to be more realistic and thus more challenging by correcting for an aberrated wavefront existing before incidence on the MMDM by fully conjugating the mirror. The challenges with this approach were that, using a random aberration can lead to wavefronts whose correction lays outside the dynamic limits of the MMDM and specifically the conjugation abilities of a mirror which was not being optimally utilized due to limitations of the apparatus.

In order to conduct this experiment, again a near perfect self-referenced wavefront was established and stored as the reference in the “Front Surfer” program. Then to create the aberrations in the wavefront, a simple, clear plastic compact disk (CD) case was placed in the path of the beam before incidence on the MMDM. The resulting wavefront

was measured and compared to the stored reference. Figure 21 (Left) shows the resulting aberrated wavefront from this plastic CD case. The feedback loop was then closed and the image resolved Figure 21 (Middle) with the corrective actuator values depicted on the right. Notice actuator number 4 saturates at its maximum value of 255 volts. This indicative of the aberrations of the CD case not being within the full dynamic range of the MMDM. The experiment was run numerous times each with similar results.

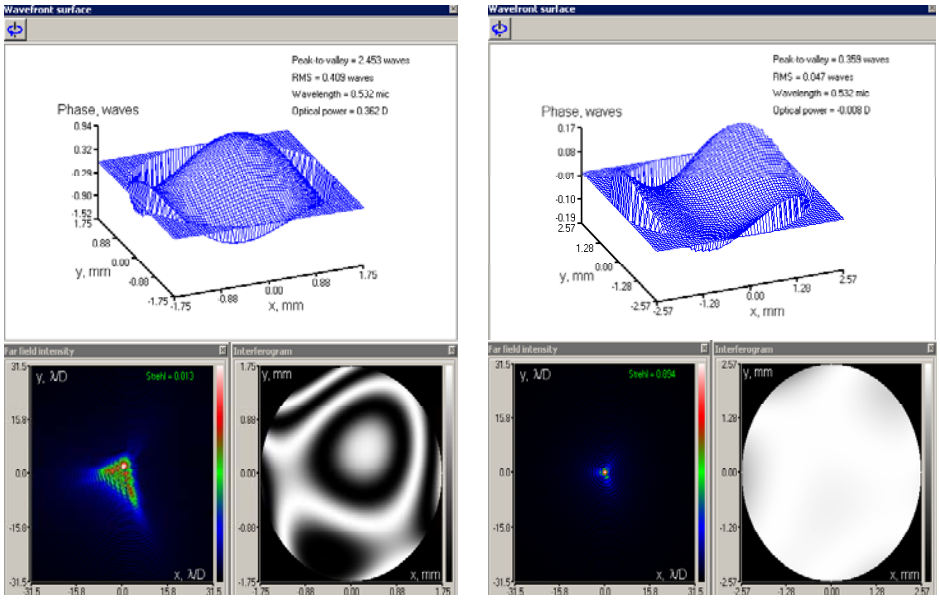

Actuator	Voltages
1	196.6324
2	154.9032
3	182.9319
4	255.2562
5	147.7274
6	158.8313
7	175.7997
8	158.8611
9	182.0017
10	178.3002
11	182.9991
12	174.9467
13	182.7571
14	190.7634
15	143.0681
16	177.8125
17	152.6872
18	168.8138

Figure 21 Aberrated wavefront (Left) caused by placing clear plastic CD case (aberrator) in front of the MMDM. (Middle) shows the resulting output (corrected) wavefront after MMDM conjugation controlled by the Phase Diversity wavefront sensor. (Right) Shows the actuator voltage values required for correction of the aberrated wavefront.

Figure 22 shows similar results for the same experiment conducted above with a different aberrator (a different plastic CD case). Again the results were conclusive that the mirror was conjugating to correct for the induced aberrations. As in the above

example, again one actuator saturated to its dynamic limit of 255 volts, but nonetheless, the wavefront was corrected from over two waves of aberration down to less than half a wave.

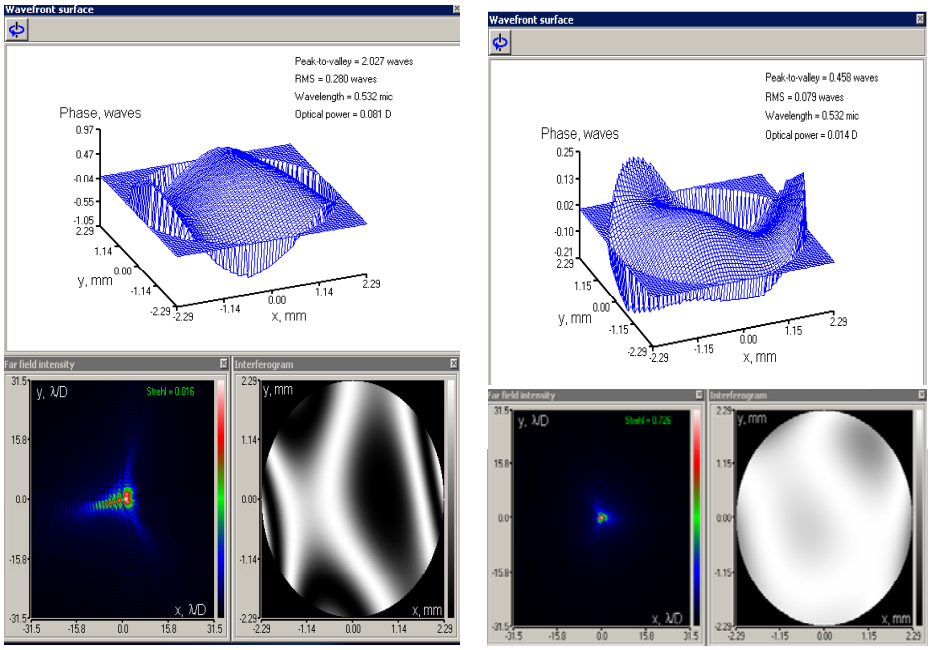

Actuator	Voltages
1	167.3530
2	234.3771
3	255.1989
4	178.1298
5	185.0272
6	186.8067
7	143.2041
8	180.2360
9	169.1133
10	179.3695
11	186.1748
12	172.8959
13	182.9836
14	162.2159
15	173.5406
16	153.0218
17	181.1846
18	175.0979

Figure 22 Same experiment as depicted in Figure 21 this time showing saturation in actuator number 3. Notice the improvement in the wavefront going from over 2 waves of aberration to less than half a wave of aberration. This experiment routinely fell short of the preferred .25λ but the significance of improvement cannot be ignored.

V. CONCLUSIONS AND FUTURE RESEARCH

A. SUMMARY OF WORK

In summary, a Phase Diversity Wavefront Sensor was built using two CMOS cameras placed equidistant on either side of focus. Knowing that an unaberrated wavefront should show no difference in the region-by-region intensity as governed by the area of actuation or disturbance caused by the movement of an actuator, a Matlab algorithm was written such that any regionally observed difference in intensity on the MMDM could be minimized by moving individual actuators to conjugate the mirror. This process served to correct the aberrated wavefront for better image resolution.

Two experiments were conducted to prove the concept. First, using three of the six actuator rings available on the MMDM, a Shack-Hartmann WFS, and the "Front Surfer" wavefront analysis and mirror control software, a reference wavefront was measured by the system. Then the deformable mirror was deliberately aberrated to over 30 waves of aberration. The Phase Diversity WFS was then given close-loop control to conjugate the MMDM using the intensity difference data it observed. Within approximately 3000 iterations or about 2.5 minutes, the PD WFS had completely conjugated the MMDM back to its reference position resolving the image 300 fold down to resolutions of approximately 1/3 wave. This experiment was repeated numerous times with similar results.

The second experiment, designed to be more realistic of actual intended use, involved creating an aberrated wavefront before incidence on the MMDM by placing a simple clear plastic CD case in front of the ideally planar reference beam (wavefront). This aberrator caused a noticeable amount of aberration of approximately two waves again using the Shack-Hartmann WFS and the "Front Surfer" program. The PD WFS was again given closed-loop control of the MMDM using the intensity difference data from the two cameras and again the systems succeeded is conjugating the MMDM for increased resolution. Typical five-fold improvements were observed and always to within one half a wave.

B. CONCLUSIONS

Though resolutions down to the limits of diffraction of .25λ were not achieved, resolutions of .3 to .45 λ were typical with wavefront improvements of up to 300 times. With future expansion of this work to include the automation of registration, such that all 59 MMDM actuators can be used, there is full confidence in the system's ability to resolve down to the optical limits of diffraction.

C. FUTURE SRDC RESEARCH

Currently the NPS Spacecraft Research and Design Center is exploring the challenges of designing space-based terrestrial imaging systems capable of high resolutions, with the ultimate objective of basing in geo-synchronous orbits. In order achieve resolutions desired and in keeping with the orbital launch weight and size limitations of such lofty goals, the problem lends to the use of large light-weight optical systems requiring adaptive optics.

As previously mentioned the SRDC AO has developed a 3-closed-loop AO system. The 1st closed-loop uses an on-board reference (unaberrated) laser beam to compare to the detected (aberrated) object beam and correct for abnormalities in the primary deformable mirror which is intended to simulate a very large, lightweight flexible membrane mirror capable of meeting the size and weight limitations for geosynchronous orbit insertion. By bouncing the reference beam off the same deformable mirror as the object beam, the reflection of the reference beam, being deformed, due to the flexible nature of the DM membrane surface is analyzed by the wavefront sensor which provides feedback through a computer such that it can apply corrections to the DM. This mostly corrected object beam image is sent to the next AO loop. This primary loop is intended to correct for low frequency aberrations. The next phase of SRDC research will replace the primary optic (currently an MMDM) with an 18 inch diameter, 6 section segmented mirror provided by Sandia National Laboratories. The wavefront sensing required to use this new primary optic will require a Phase Diversity system to provide wavefront continuity across segment edges and compensate for mirror piston.

After low frequency correction by the primary AO loop the object and reference beams travel on to the second correction loop to compensate for jitter (tip and tilt) onboard the spacecraft itself. This second closed loop system is identical to the first save it uses a fast steering mirror and a position sensing device (PSD) as the sensor to remove both tip and tilt.

Jitter is a common issue onboard spacecraft which use slewing mechanisms where vibrations caused by the slewing maneuver itself must be compensated.

Once both onboard jitter and low frequency aberrations have been corrected in the first two loops, the object beam continues alone to the third loop. Here, a second DM and WFS are used to remove any remaining high frequency aberrations in the object beam. It is important to note that this final loop requires some reference for which to compare the object beam in order to apply corrections. This reference can come from either another referencing guide laser or from the glint (reflection) of a known object within the field of view of the object beam.

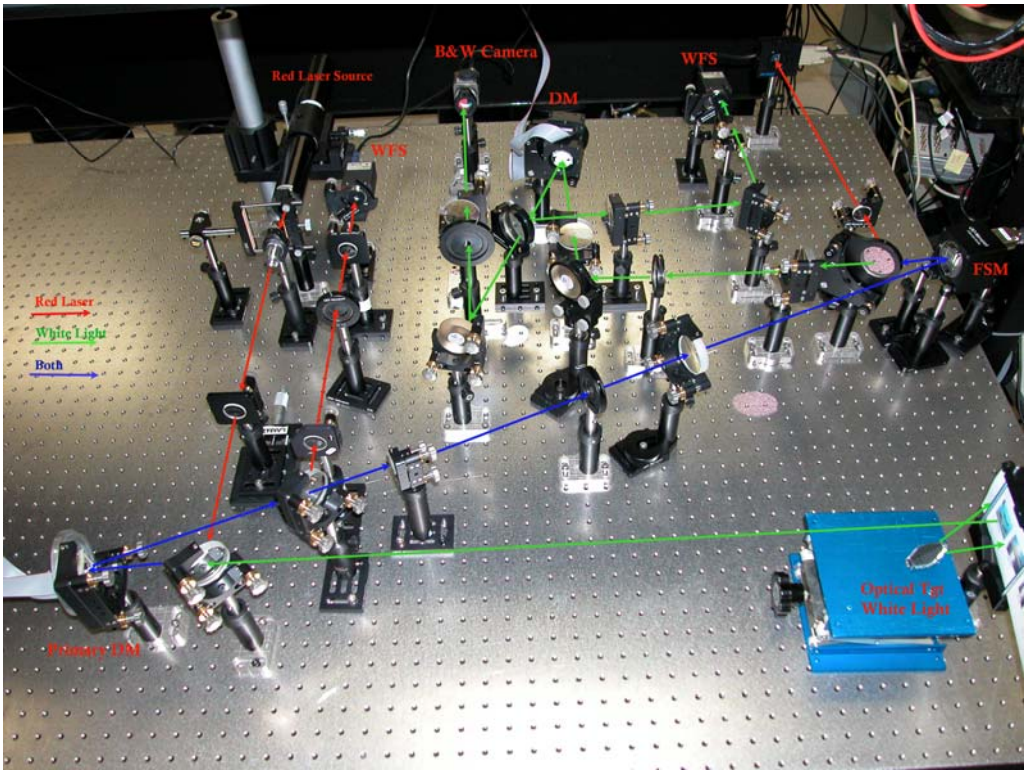

Figure 23 Photo of the SRDC 3-Loop AO Test bed with current MMDM primary in place.

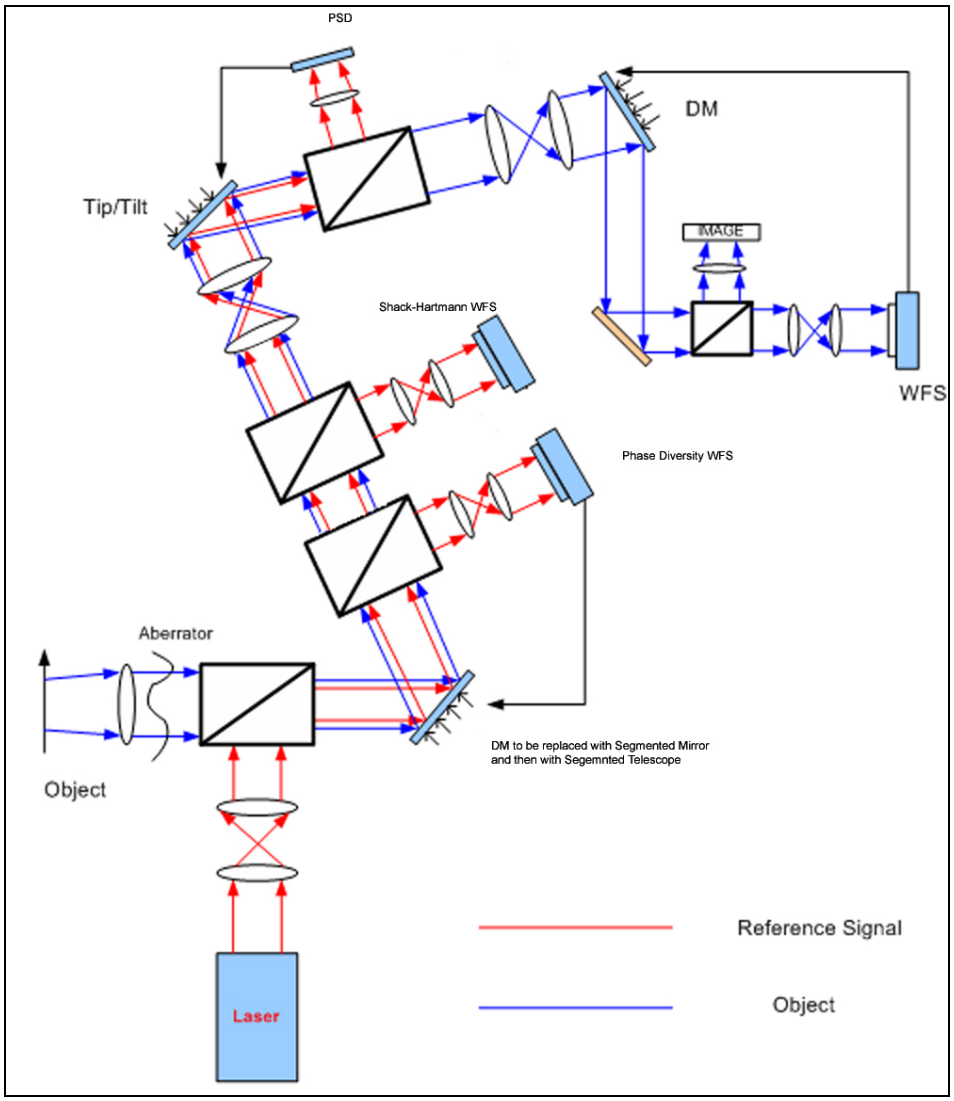

Figure 24 SRDC basic 3-Loop AO system diagram showing the implementation of a Phase Diversity WFS system in the primary correction loop.

In the near term, the Phase Diversity system will be fully implemented into the SRDC's 3-loop AO system as shown in Figure 24 The PD system will require a full registration of all actuators or segments when using the new Sandia segmented mirror. Additionally, once fully implemented, a better (dedicated Shack-Hartmann WFS will be used such that PD data can be compared. This will undoubtedly provide for a more refined analysis of the capability of the system and optimization of the control algorithms necessary for the research objectives.

MATLAB SCRIPT APPENDIX

```
Mirror Control

 % set initial voltage to the mirror
%This routine was used to set the MMDM to its neutral bias condition
such %that a reference (background) image could be generated subtracted
out thus %removing that noise and those aberrations inherent in the
system
V = ones(1,59)*180.31222;
V(1:18)=180.31222;
V(19:59)=180.31222;
BAODMirror59(hex2dec('D800'),hex2dec('D400'),hex2dec('D000'),V);
%D800, D400, and D000 were the data addresses of the MMDM control
boards in the computer.

% starting the control loop
for i=1:5000;
    % read voltage values from the other computer.  This allowed the
mirror %control computer to access PD intensity data via a share drive
with the PD %WFS control computer.
fid=fopen('C:\Documents and Settings\All
Users\Documents\voltage_data.txt','r');
    if fid~=-1
        partialV = str2num(fread(fid,'*char')');
        fclose(fid);
        if length(partialV) == 18
            deltaV = [partialV zeros(1,41)];
           %Simple control law applied to the 1st 3 rings of actuators
only
            K = .1;
            V = V-K*deltaV;
            V(1:18)
            for i=1:length(V)
                if V(i) >=255
                    V(i) = 255;
                elseif V(i) <=0
                    V(i) = 0;
                else
                    V(i) = V(i);
                end
            end

BAODMirror59(hex2dec('D800'),hex2dec('D400'),hex2dec('D000'),V);
        end
    end
end
```

Phase Diversity Wavefront Sensor

```
%This program was used to slave one camera to the other in
data %collection.

%Map2ImagesSlaveC2.m--Run this program first on a Separate Matlab...

if(exist('Camera2.bin')==0); %create this file if it does not yet exist
    %Stuff for creating the memory mapped file in the first place for
later use
    %It doesn't matter what is in the file, it just has to exist
    fid=fopen('Camera2.bin','w');%open the 2nd camera file for creation
    fake=zeros(1024,1024,'uint8');%create fake image data
    fwrite(fid,fake,'uint8');%write fake data into file, which will be
used for mapping
    fclose(fid);
end
m=memmapfile('Camera2.bin','format',
{'uint8',[1024,1024],'C2'},'writable',true);
Camera2=m.Data.C2;%reads data out of Camera2 variable
monograbC2(0);%initialize frame grabber#2
while 1==1;
    m.Data.C2=monograbC2(1);%stuff the memory-mapped file continuously
with images
end
monograbC2(2);clear monograbC2;%this will never get executed, actually
```

Phase Diversity Wavefront Sensor Continued

```
%This program was used to control the master camera and pull its data
for analysis

%Map2ImagesMasterBothC1andC2.m

if(exist('Camera2.bin')==0); %create this file if it does not yet exist
    %Stuff for creating the memory mapped file in the first place for
later use
    %It doesn't matter what is in the file, it just has to exist
    fid=fopen('Camera2.bin','w');%open the 2nd camera file for creation
    fake=zeros(1024,1024,'uint8');%create fake image data
    fwrite(fid,fake,'uint8');%write fake data into file, which will be
used for mapping
    fclose(fid);
end
m=memmapfile('Camera2.bin','format',
{'uint8',[1024,1024],'C2'},'writable',true);

load HOT_PIX_DATA

% monograbC1(0);%initialize frame grabber#2
for i=1:5;
 monograbC1(0);
    Camera1=monograbC1(1);
    Camera2=m.Data.C2;%reads data out of Camera2 variable
    Camera2=flipud(Camera2);

 C1=double(Camera1);
 C2=double(Camera2);

%  This section was used only to produce the hot pixel matrix and was
left %commented out after the hot pixel data was saved to be loaded for
future %iterations.
%     HOTC1=C1(400:800,300:700);
%      HOTC2=C2(400:800,300:700);
%   for i=1:401;
%       for j=1:401;
%           if HOTC1(i,j)>50;
%              HOTC1(i,j)=0;
%           else HOTC1(i,j)=1;
%           end
%       end
%   end
%    for i=1:401;
%       for j=1:401;
%           if HOTC2(i,j)>50;
%              HOTC2(i,j)=0;
%           else HOTC2(i,j)=1;
```

```
%           end
%       end
%    end
%  end
%  HOT_PIX_DATA =HOTC1, HOTC2;
%  save HOT_PIX_DATA

%Remove unused pixel data (reduction form 1024x1024 to 400x400)
C1=C1(400:800,300:700);
C2=C2(400:800,300:700);


%removing hot pixels
C1=C1.*HOTC1;
C2=C2.*HOTC2;

%elimination of noise
for i=1:401;
       for j=1:401;
           if C1(i,j)<20;
              C1(i,j)=0;
           end
       end
   end
    for i=1:401;
       for j=1:401;
           if C2(i,j)<20;
              C2(i,j)=0;
           end
       end
    end


%smoothing the intensity data through convolution
     F=[.125 .25 .125; .25 1 .25; .125 .25 .125];
     C1 = conv2(C1,F,'same');
     C2 = conv2(C2,F,'same');
     C1 = conv2(C1,F,'same');
     C2 = conv2(C2,F,'same');
% %
    C1max=max(max (C1))
    C2max=max(max (C2))

% %Scaleing the data to keep all positive values when subtracting
intensity %differences
    C2scaled=C2*mean(mean(C1))/mean(mean(C2));
    C1scaled=C1*mean(mean(C2))/mean(mean(C1));
    C2scaledmax=max(max(C2scaled));

%plotting the camera 1 image, camera 2 image, and the difference of
each one %from the other, scaled for intensity normalization and with
background %reference image subtracted out.
figure(1);
  subplot(2,2,1);imagesc(C1scaled);axis image;colormap (gray);colorbar;
```

```
    subplot(2,2,2);imagesc(C2scaled);axis image;colormap
(gray);colorbar;
    subplot(2,2,3); imagesc((C2scaled-C1scaled)-min(min(C2scaled-
C1scaled+DC0))+DC0);axis image;colormap (gray (256));colorbar;
    subplot(2,2,4); imagesc((C1scaled-C2scaled)-min(min(C1scaled-
C2scaled-DC0))-DC0);axis image;colormap (gray (256));colorbar;

%building the phase diversity intensity difference matrix to be saved
and iterated in the control loop.
    pd_data= C1-C2scaled;
    [bs_index_x,bs_index_y] = find(pd_data == max(max(pd_data)));

 monograbC2(2);
 clear monograbC2;

% find noisy spots and set to zero
[indx,indy] = find(check<20);% for voltages less than 180
%[indx,indy] = find(check>-40);% for voltages grater than 180
for i = 1:length(indx)
check(indx(i),indy(i)) = 0;
end

% find dark areas and conpute sume and centroid
[indx,indy] = find(check~=0);
summ = 0;Rx = 0;Ry = 0;
for i = 1:length(indx)
summ = summ + check(indx(i),indy(i));
Rx = Rx+indx(i)*check(indx(i),indy(i));
Ry = Ry+indy(i)*check(indx(i),indy(i));
end

% compute average value
if length(indx)==0,
    mean_check = 0;
    C_x = 0;
    C_y = 0;
else
    mean_check = summ/length(indx);
    C_x = Rx/summ;
    C_y = Ry/summ;
end

% % plot only good data points
 figure(3);imagesc(check);axis image;colormap (gray (256));colorbar;
end
% creating a box around centroid
xspan = [round(C_x)-10:round(C_x)+10];
yspan = [round(C_y)-10:round(C_y)+10];
boxdata = pd_data(xspan,yspan) - DC0(xspan,yspan);

% compute the average intensity in the box
avg_box = sum(sum(boxdata))/(length(xspan)*length(yspan));

% compute tension constant
```

```
delV = -10;
Const = avg_box/delV;
%
```

This program was used to send the PD data to the share computer to drive the mirror control.

```
%Map2ImagesMasterBothC1andC2.m

if(exist('Camera2.bin')==0); %create this file if it does not yet exist
    %Stuff for creating the memory mapped file in the first place for
later use
    %It doesn't matter what is in the file, it just has to exist
    fid=fopen('Camera2.bin','w');%open the 2nd camera file for creation
    fake=zeros(1024,1024,'uint8');%create fake image data
    fwrite(fid,fake,'uint8');%write fake data into file, which will be
used for mapping
    fclose(fid);
end
m=memmapfile('Camera2.bin','format',
{'uint8',[1024,1024],'C2'},'writable',true);

load HOT_PIX_DATA
load CENTROID_DATA


% monograbC1(0);%initialize frame grabber#2 sets the number of control
loop iterations to process.
for i=1:1000;
 monograbC1(0);
    Camera1=monograbC1(1);
    Camera2=m.Data.C2;%reads data out of Camera2 variable
    Camera2=flipud(Camera2);

 C1=double(Camera1);
 C2=double(Camera2);


C1=C1(400:800,300:700);
C2=C2(400:800,300:700);


           C1=C1.*HOTC1;
           C2=C2.*HOTC2;
%Sets the noise level to exclude data inside the noise thresh hold.
for i=1:401;
       for j=1:401;
           if C1(i,j)<10;
              C1(i,j)=0;
           end
```

```
        end
    end
     for i=1:401;
        for j=1:401;
            if C2(i,j)<10;
               C2(i,j)=0;
            end
        end
     end


     C2scaled=C2*mean(mean(C1))/mean(mean(C2));


      pd_data= C1-C2scaled;

%sets the number of actuators used in the iteration 18 of
59 here.
for i = 1:18
C_x = C_data(i,1);C_y = C_data(i,2);
xspan = [round(C_x)-10:round(C_x)+10];yspan = [round(C_y)-
10:round(C_y)+10];
boxdata = pd_data(xspan,yspan) - DC0(xspan,yspan);
avg_box(i) = sum(sum(boxdata))/(length(xspan)*length(yspan));
end

Const = -3.5;
voltage_data = avg_box'/Const;
data_str = [];
for i = 1:length(voltage_data);
    data_str = [data_str, ' ',num2str(voltage_data(i))];
end

fid = fopen('\\CONTROLFREAK_1\SharedDocs\voltage_data.txt', 'w');
if fid ~= -1
    fwrite(fid, data_str, 'char');
    fclose(fid);
end

end
```

THIS PAGE INTENTIONALLY LEFT BLANK

LIST OF REFERENCES

Andrews, J., Restaino, S. R., Dynamic Aberration Control Test bed for the Characterization of Multiple Wavefront Sensors, University of New Mexico, Undated. Naval Research Laboratory, Remote Sensing Division, Albuquerque NM.

Born, M. and Wolf E. (1999). Principles of Optics, (7th ed.). United Kingdom: Cambridge University Press.

Burley, G. S., Stilburn, J. R., and Walker, G. A. H. (1998). Membrane Mirrors and Bias Electronics, Journal of Applied Optics, Optical Society of America, 20 July 1998, Vol. 37, No. 21.

Bush, K., Marrs, A., and Schoen, M., (2006). Electrostatic Membrane Deformable Mirror Characterization and Applications, AgilOpics Inc. Albuquerque NM.

Campbell, H. I., Zhang, S., Greenaway, A. H. and Restaino, S. R. (2004). Generalized Phase Diversity for Wavefront Sensing, Optics Letters, Optical Society of America, Vol. 29, No. 23, 1 December 2004.

CFAO (2007), Center for Adaptive Optics Summer program lecture series, http://cfao.ucolick.org/aosummer/archive/aosummer2004/lectures.php, 19 Nov 07.

CTIO (2006), Cerro Tololo Inter-American Observatory, Online Adaptive Optics Tutorial, http://www.ctio.noao.edu/~atokovin/tutorial/intro.html, December 2006.

Hecht, E. (2001). Optics (4th ed.). San Francisco, CA: Addison Wesley.

Heriot Watt University, (2007). Website, Adaptive Optics Theory. http://waf.eps.hw.ac.uk/Theory%20Pages/Adaptive%20Optics%20Theory%20Page.htm, 19 Nov 2007.

Löfdahl, M. G., (1996). Phase diversity wavefront sensing and image restoration applied to high-resolution solar observations. Royal Swedish Academy of Sciences, Stockholm Observatory.

OKO (2006). Adaptive Optics Product Guide, Flexible Optical BV (OKO Technologies).

Restaino, S. R., (Undated). High Angular Resolution, University of New Mexico Class Notes, Undated. Naval Research Laboratory, Remote Sensing Division, Albuquerque NM.

Rochester, University of Rochester Astronomy 203/403 Lecture Series, Fall 1999, http://www.pas.rochester.edu/~dmw/ast203/Lectures.htm, December 2006.

Roddier, F., (1999). Adaptive Optics in Astronomy, United Kingdom: Cambridge University Press.

Roddier, C., Roddier F., (1993). Wavefront Reconstruction from Defocused Images and the Testing of Ground-based Optical Telescopes. Optical Society of America, Vol. 10, No. 11, November 1993.

Roddier, C., Roddier F., (1988). Curvature Sensing and Compensation; A new concept in Adaptive Optics, Appl. Opt. 27, pp 1223-1225.

Talmi, A., Ribak, E. (2006), Wavefront Reconstruction from its Gradients, Journal of the Optical Society of America, Vol.23, No. 2, Febuary 2006.

Tyson, R. K., (1998). Principles of Adaptive Optics, (2nd ed.). San Diego CA: Academic Press.

Tyson, R K., (2000). Introduction to Adaptive Optics, SPIE Press.

Tyson, R. K. and Frazier B. W., (2004). Field Guide to Adaptive Optics,. Bellingham WA: SPIE Press.

Van Dam, M. A. and Lane, R. G., (2002). Extended Analysis of Curvature Sensing. Optical Society of America, Vol. 19, No. 7, July 2002.

Yang, Q., Ftaclas, C., and Chun, M., (2006). Wavefront Correction with High-order Curvature Adaptive Optics Systems. Journal of the Optical Society of America, Vol. 23, No. 6, June 2006

INITIAL DISTRIBUTION LIST

1. Defense Technical Information Center
   Ft. Belvoir, Virginia

2. Dudley Knox Library
   Naval Postgraduate School
   Monterey, California